



HAL
open science

On the reversibility of membrane fouling by deposits produced during crossflow ultrafiltration of casein micelle suspensions

Maksym Loginov, Floriane Doudières, Nicolas Hengl, Mohamed Karrouch, Nadine Leconte, Fabienne Garnier-Lambrouin, Javier Pérez, Frédéric Pignon, Geneviève Gésan-Guiziou

► To cite this version:

Maksym Loginov, Floriane Doudières, Nicolas Hengl, Mohamed Karrouch, Nadine Leconte, et al.. On the reversibility of membrane fouling by deposits produced during crossflow ultrafiltration of casein micelle suspensions. *Journal of Membrane Science*, 2021, 630, pp.119289. 10.1016/j.memsci.2021.119289 . hal-03199144

HAL Id: hal-03199144

<https://hal.inrae.fr/hal-03199144>

Submitted on 15 Apr 2021

HAL is a multi-disciplinary open access archive for the deposit and dissemination of scientific research documents, whether they are published or not. The documents may come from teaching and research institutions in France or abroad, or from public or private research centers.

L'archive ouverte pluridisciplinaire **HAL**, est destinée au dépôt et à la diffusion de documents scientifiques de niveau recherche, publiés ou non, émanant des établissements d'enseignement et de recherche français ou étrangers, des laboratoires publics ou privés.



Distributed under a Creative Commons Attribution - NonCommercial - NoDerivatives 4.0 International License



On the reversibility of membrane fouling by deposits produced during crossflow ultrafiltration of casein micelle suspensions

Maksym Loginov^{a,*}, Floriane Doudières^{a,b}, Nicolas Hengl^b, Mohamed Karrouch^b, Nadine Leconte^a, Fabienne Garnier-Lambrouin^a, Javier Pérez^c, Frédéric Pignon^b, Geneviève Gésan-Guizou^a

^a STLO, INRAE, Institut Agro, 35042, Rennes, France

^b Univ. Grenoble Alpes, CNRS, Grenoble INP (Institute of Engineering Univ. Grenoble Alpes), LRP, F-38000, Grenoble, France

^c SWING Beamline, SOLEIL Synchrotron, 91192, Gif-sur-Yvette, France

ARTICLE INFO

Keywords:

Membrane fouling
Deposit irreversibility
Gel swelling
Compression-permeability
Filtration model

ABSTRACT

The formation of a deposit layer on membrane surfaces is an important problem, particularly in milk filtration. Properties of the deposit and efficiency of deposit removal can be studied using various indirect methods based mainly on average membrane resistance in deposit formation–deposit removal cycles, but their conclusions on deposit reversibility depend on conditions surrounding deposit analysis.

Here we present a method for direct characterization of the reversibility of deposit compression via analysis of local solid concentration distribution during deposit formation at constant pressure and cross-flow velocity and deposit removal after pressure relaxation. Two models are proposed for deposit characterization: a model of crossflow filtration with deposit formation to characterize deposit compressibility-permeability from the data on concentration distribution at steady-state of deposit formation, and a model for evaluating deposit swelling kinetics from the data on steady-state compressibility-permeability.

The method was applied here for analysis of the deposit formed on the surface of a polymeric ultrafiltration membrane during crossflow filtration of casein micelle suspensions at 25°C. Local solid concentration distribution in the deposit and concentration polarization layer was probed *in situ* using small-angle X-ray scattering (SAXS). Experiments were performed in a special-purpose SAXS–filtration cell. It was demonstrated that casein micelle deposits obtained at 1.1 bar transmembrane pressure swell after pressure relaxation. However, swelling rate was significantly lower than that obtained by modeling using deposit compressibility–permeability obtained from the analysis of steady-state concentration distribution. We thus find evidence that casein micelle deposits produced during crossflow membrane filtration undergo compression that is partially irreversible.

1. Introduction

The build-up of colloidal deposit on the membrane surface during skim milk microfiltration reduces the permeate flux as well as the transmission of serum proteins into the filtrate, and can complicate membrane regeneration by rinsing [1]. This problem becomes more acute when microfiltration is performed using polymer membranes in spiral-wound modules, as the equipment does not allow a sufficiently high wall shear stress (which could increase particle back-transport, reduce deposit formation and improve deposit removal) and may degrade at high temperature (which could decrease retentate viscosity

and improve the efficiency of chemical membrane cleaning). To address this issue, a number of articles on milk filtration have set out to identify operating conditions that drive deposit formation (shear stress, transmembrane pressure, etc.) [1,2].

Conventional methods for studying deposit formation usually employ stepping (cycled variation) of operating parameters such as permeate flux, shear stress or transmembrane pressure [1,3–5] and characterize membrane fouling with average values of clean, fouled and rinsed membrane resistances [1,6] or, more rarely, the local membrane resistance [7–10]. In this case, any significant increase in membrane fouling rate is attributed to deposit formation, which is considered ‘irreversible’ if fouled membrane resistance does not decrease or fails to

Abbreviations: CP, concentration polarization; E, erosion step (experimental); F, filtration step (experimental); R, pressure relaxation step (experimental); SAXS, small-angle X-ray scattering; UF, ultrafiltration.

* Corresponding author.

E-mail address: maksym.loginov@inrae.fr (M. Loginov).

<https://doi.org/10.1016/j.memsci.2021.119289>

Received 18 October 2020; Received in revised form 4 March 2021; Accepted 20 March 2021

Available online 29 March 2021

0376-7388/© 2021 Elsevier B.V. All rights reserved.

Nomenclature	
a	length of the filtering part of a cross-section of the filter channel; width of the filter channel of the SAXS-filtration cell (m)
c	casein concentration ($\text{kg} \cdot \text{m}^{-3}$)
c_0	casein concentration in filtered suspension ($\text{kg} \cdot \text{m}^{-3}$)
c_{sg}	casein concentration in the point of sol-gel transition ($\text{kg} \cdot \text{m}^{-3}$)
c_m	solid (i.e. casein) concentration on the membrane surface ($\text{kg} \cdot \text{m}^{-3}$)
h_{CP}	local thickness of the CP layer (m)
h_g	local thickness of the gel layer (deposit) (m)
I_{tr}	intensity of the transmitted X-ray beam (arbitrary units)
$J(x)$	local filtrate flux at the distance x from the entrance to the filter channel ($\text{m} \cdot \text{s}^{-1}$)
$J(0)$	filtrate flux at the entrance to the filter channel ($x = 0$ cm) ($\text{m} \cdot \text{s}^{-1}$)
J_0	filtrate flux across the clean membrane ($\text{m} \cdot \text{s}^{-1}$)
J_L	average filtrate flux over the filter channel ($\text{m} \cdot \text{s}^{-1}$)
$J_{L,ss}$	average filtrate flux over the filter channel at steady-state filtration ($\text{m} \cdot \text{s}^{-1}$)
k	local hydraulic permeability (m^2)
L	length of the filter channel (m)
M	filterability, material property that governs crossflow filtration ($\text{Pa}^3 \cdot \text{m}^2 \cdot \text{s}$)
m_g	quantity of excess casein in the deposit (gel layer) ($\text{g} \cdot \text{m}^{-2}$)
m_t	total quantity of excess casein in the fouling layer ($\text{g} \cdot \text{m}^{-2}$)
P	total pressure in the filtration channel (Pa)
P_0	total pressure at the entrance to the filter channel (Pa)
ΔP	transmembrane pressure (Pa)
ΔP_R	pressure applied during relaxation (Pa)
p_s	local compressive solid pressure (Pa)
Q	average tangential flow in the filter channel ($\text{m}^3 \cdot \text{s}^{-1}$)
Q_0	average tangential flow at the entrance to the filter channel ($\text{m}^3 \cdot \text{s}^{-1}$)
R	membrane radius (when the filter channel is cylindrical) (m)
R_f	average hydraulic resistance of fouled membrane at steady-state filtration (m^{-1})
R_m	hydraulic resistance of the membrane during deposit swelling at the pressure relaxation step (m^{-1})
R_{m0}	hydraulic resistance of clean membrane (m^{-1})
R_r	average hydraulic resistance of the membrane attained after rinsing, hydraulic resistance of the membrane with residual fouling (m^{-1})
t	time (min)
t_E	erosion time (min)
t_F	filtration time (min)
t_R	relaxation time (min)
u	local crossflow (tangential) velocity ($\text{m} \cdot \text{s}^{-1}$)
u_{av}	average crossflow velocity ($\text{m} \cdot \text{s}^{-1}$)
x	axial (horizontal) distance from the entrance to the filter channel (m)
y	lateral coordinate, distance from the central plane (m)
z	normal (vertical) distance from the membrane surface (m)
<i>Greek letters</i>	
$\dot{\gamma}$	local shear rate (s^{-1})
μ_f	filtrate viscosity ($\text{Pa} \cdot \text{s}$)
Π	local osmotic pressure of particles (micelles) in the CP layer (or solid pressure in the gel/deposit) (Pa)
ρ_s	density of solid ($\text{kg} \cdot \text{m}^{-3}$)
τ	shear stress (Pa);
τ_w	wall shear stress (Pa);
v	voluminosity of casein micelles ($\text{ml} \cdot \text{g}^{-1}$);
ϕ_{sg}	volume fraction of casein micelles in the point of sol-gel transition (dimensionless);
ω	material coordinate (m)

attain its starting value at the end of the cycle (i.e. the deposit or its part remains on the membrane surface). The cited methods are not, therefore, focused on direct characterization of deposit properties, so their conclusions on the ‘irreversibility’ of deposit formation remain specific to the stepping conditions applied (which nevertheless has great practical importance for the filtration equipment used).

Note that any common characterization of deposit irreversibility is by definition arbitrary, as deposits produced during milk filtration can be removed by proper rinsing [11] (although the required hydrodynamic conditions, rinse time and mechanism of deposit removal are generally unknown). Moreover, deposit removal is a dynamic process (as shown for microfiltration of milk proteins in e.g. Refs. [12,13]). Therefore, deposit irreversibility can only strictly be characterized by correlating the timescale of the experiment with a characteristic timescale of deposit evolution [14] (swelling, redispersion, etc.), which builds on the idea of using the Deborah number to characterize membrane fouling [15]. Proper characterization of deposit irreversibility therefore requires knowing key properties of the deposit and its removal mechanism that can be further recalculated into the characteristic removal time.

According to Ref. [16], deposit formation in milk filtration is caused by casein micelles, which are soft colloidal particles with diameter ranging from 50 nm to 500 nm and an average diameter of about 150–200 nm. The micelles get deformed and compressed into a deposit under the applied osmotic or compressive pressure, then expand back to their initial size after the pressure is released (in the range of pressures applied in milk filtration) [17,18]. Casein micelles are core-shell

particles with a hydrophilic polymeric brush of κ -caseins on the surface that provides a steric and electrostatic barrier against aggregation in diluted dispersions. The potential irreversibility of casein micelle deposits could arise from suppression of this barrier [18] or even the expression of non-covalently-bonded κ -caseins from the micelle surface [19].

Deposit formation is generally explained by the model of particle aggregation at the membrane surface [20–23]: the deposit appears on the membrane surface when the local particle concentration (osmotic pressure, solid compressive pressure) in the concentration polarization layer exceeds sol-gel transition concentration. Unfortunately, this model does not account for particle elasticity or compressible steric barrier (i.e. for the possibility of deposit swelling and redispersion). It has been used to demonstrate deposit formation in experiments on dead-end filtration of casein micelle dispersions, where the deposit emerged when pressure on the membrane surface exceeded a critical value [17]. The deposit was detected as the appearance of residual fouling resistance after the pressure release and mild rinsing at the end of filtration cycle [17], and deposit swelling was evidenced from the decrease of residual fouling resistance after the pressure release [17]. The reversibility (i.e. potential redispersion) of concentrated casein micelles was studied in *ex situ* experiments on osmotic compression and swelling of casein micelle dispersions [18]. These experiments demonstrated that casein micelle gels can swell after the pressure release and attain an average concentration that is lower than the sol-gel transition concentration, while remaining solid. This implies that casein micelles can aggregate by compression [18]. Redispersion of casein micelles was

observed simultaneously with the gel swelling (and in the absence of external shear), which suggests that the micelles may lose cohesion with time [18]. Casein micelle deposits in filtration are therefore likely to show a complex pattern of evolution that depends on pressure, shear and time. Unfortunately, the swelling kinetics and properties of casein micelle gels (neither that of swelling casein micelle deposits) were not strictly characterized in previous studies.

There are few studies addressing the quantitative characterization of colloidal deposit and their *in situ* behavior after the filtration pressure release (e.g. Refs. [17,24,25]), largely due to the difficulty involved in analyzing deposition on the membrane surface. However, a rigorous method for characterizing swelling behavior has been developed as part of basic filtration theory for macroscopic filter cakes that measures equilibrium particle concentration after the release of compressive pressure [26–28]. A similar approach can be applied in membrane filtration, not only during deposit formation [29] but also after pressure release, if the particle concentration in the swelling deposit can be measured.

Various (instrumentally sophisticated) methods can be applied for local deposit analysis in membrane filtration [30,31]. An *in situ* small-angle X-ray scattering (SAXS)–filtration method [32–34] has successfully visualized deposit growth and erosion by crossflow or ultrasound for casein micelles [34,35] and other nanocolloids [36,37]. The method enables simultaneous measurement of the average filtrate flux and local solid concentration at different distances from the membrane surface with a spatial resolution of 20 μm [38–40]. It can also serve to analyze deposit behavior after the pressure release and to characterize deposit reversibility. For example, in a recent paper on SAXS-ultrafiltration of casein micelle suspensions at the constant pressure of 110 kPa [62] we proposed a method for semi-quantitative analysis of deposit swelling and removal and compared the influence of filtration temperature (12°C versus 42°C) on the deposit compressibility and its swelling kinetics during the pressure relaxation. Our current work continues the development of methodology for characterization of deposit properties with a focus on reversibility of deposit formation and compression.

Here we report new work characterizing deposits produced during crossflow ultrafiltration of casein micelle dispersions. *In situ* SAXS is used to measure local casein concentration in the concentration polarization layer and deposit during deposit formation at different transmembrane pressures and at subsequent filtration pressure release (relaxation), as well as the increase in average crossflow velocity (erosion). A new method is developed for quantitative characterization of deposit compressibility–permeability. We also compare different methods for characterizing the reversibility of membrane foulant deposits: (i) a conventional method based on analysis of average membrane resistance (hydraulic resistance of fouled membrane at steady-state versus hydraulic resistances of clean membrane and rinsed membrane), and (ii) a novel method based on analysis of deposit swelling kinetics.

2. Materials and methods

2.1. Casein micelle suspensions

Casein micelle suspensions at casein concentration $c = 2\text{--}180 \text{ g}\cdot\text{l}^{-1}$ were prepared by thoroughly mixing (15 h at 35°C) casein isolate powder Promilk 852B (provided by Ingredia, Arras, France) with a skim milk ultrafiltrate (UF permeate prepared at the STLO laboratory, free of proteins and other pore blocking foulants). Detailed compositions of the raw materials can be found in Supplementary data (Table S1). The particle size distribution of the suspensions obtained was in the range 50–450 nm with an average diameter of 130 nm (measured via dynamic light scattering analysis using a Zetasizer Nano ZS sizing system, Malvern Instruments, UK), and pH was 6.7 ± 0.1 at 20°C. Particle size distribution and pH were close to those of fresh skim milk, and

redispersion reproduced the main properties of casein micelles (see Refs. [41,42]). Suspensions were preserved by addition of 0.05 wt% sodium azide (Sigma-Aldrich, St. Louis, MO) and were used within 24 h after preparation. Exact concentrations of the suspensions were calculated from their dry matter content measured by the weight method.

2.2. Filtration materials and equipment

Filtration experiments were done at 25°C with casein micelle suspension at $c_0 = 49 \text{ g}\cdot\text{l}^{-1}$.

The experiments were performed using a lab-scale crossflow SAXS–filtration rig purpose-designed for *in situ* observation of external membrane fouling. The rig is depicted in Fig. 1 and described in detail elsewhere [34,36].

The transparent polycarbonate filtration cell consisted of the upper retentate part and the lower filtrate part with a flat horizontal (parallel to the x axis) sheet of polymer membrane sandwiched between them (Fig. 1b). The membrane was placed on a perforated support plate to minimize displacement in the z direction. The retentate channel was width $a = 4 \text{ mm}$, height 8 mm, and length $L = 10 \text{ cm}$.

The polyethersulfone membrane (provided by Orelis Environnement, France) had a nominal molecular weight cut-off of 100 kDa and a working surface area of $4 \cdot 10^{-4} \text{ m}^2$. Fresh membrane (pre-soaked in the UF permeate) was used in each experiment.

2.3. SAXS-filtration experiments and analysis of local membrane fouling

Analysis of local external membrane fouling (i.e. distribution of casein concentration at the membrane surface, $c(z)$) was based on the fact that the absolute scattering intensity $I(q)$ of casein micelle dispersions is directly related to c in the q range corresponding to the form factor of the casein micelles [32–34].

Filtration experiments with *in situ* SAXS analysis of the fouling layer were performed on the SWING beamline at the French national synchrotron facility (SOLEIL, Gif-sur-Yvette, France). The 0.1 nm-wavelength incident X-ray beam was collimated to full width at half maximum of 20 μm in the z axis and 150 μm in the x axis to get highly spatially-resolved analysis of $c(z)$. Sample-to-detector distance was fixed at 3 m, which provided a scattering vector q range spanning from 0.05 nm^{-1} to 3 nm^{-1} .

Prior to filtration, the empty filter cell was fixed onto a motorized stage and the membrane surface at $x = 5 \text{ cm}$ was aligned parallel to the incident beam (under the applied compressed air pressure of 0.5 or 1.1 bar). This also allowed to determine membrane surface position $z = 0 \mu\text{m}$ with an uncertainty of 20 μm (as shown in Fig. 1c).

The system was filled with casein micelle suspensions primed at 25°C for at least 30 min. The SAXS–filtration experiments consisted of three steps (Table 1).

The parameters of filtration and pressure relaxation stages (i.e. rather low value of cross-flow velocity; lower than that applied in industrial filtration) were chosen in order to promote thick deposit formation that enabled analysis of deposit properties and behavior (this approach is frequently applied for *in situ* analysis of membrane fouling by deposit).

At the first filtration step, the fouling layer was produced at constant applied pressure and crossflow velocity. At the following pressure relaxation step, we observed the swelling and thinning of the fouling layer after significant pressure reduction. At the final erosion step, we studied the cohesiveness of the swelled layer after a fivefold increase in crossflow velocity (and wall shear stress). Wall shear stress values and other hydrodynamic parameters estimated for different stages of the experiment can be found in Supplementary data, Table S2.

During the experiment, the filter cell was periodically translated in the z axis such that the retentate channel was scanned with the incident X-ray beam from $z = 0$ (membrane surface) up to 2 mm (bulk suspension) at a constant distance from the entrance $x = 5 \text{ cm}$ (i.e. at the middle

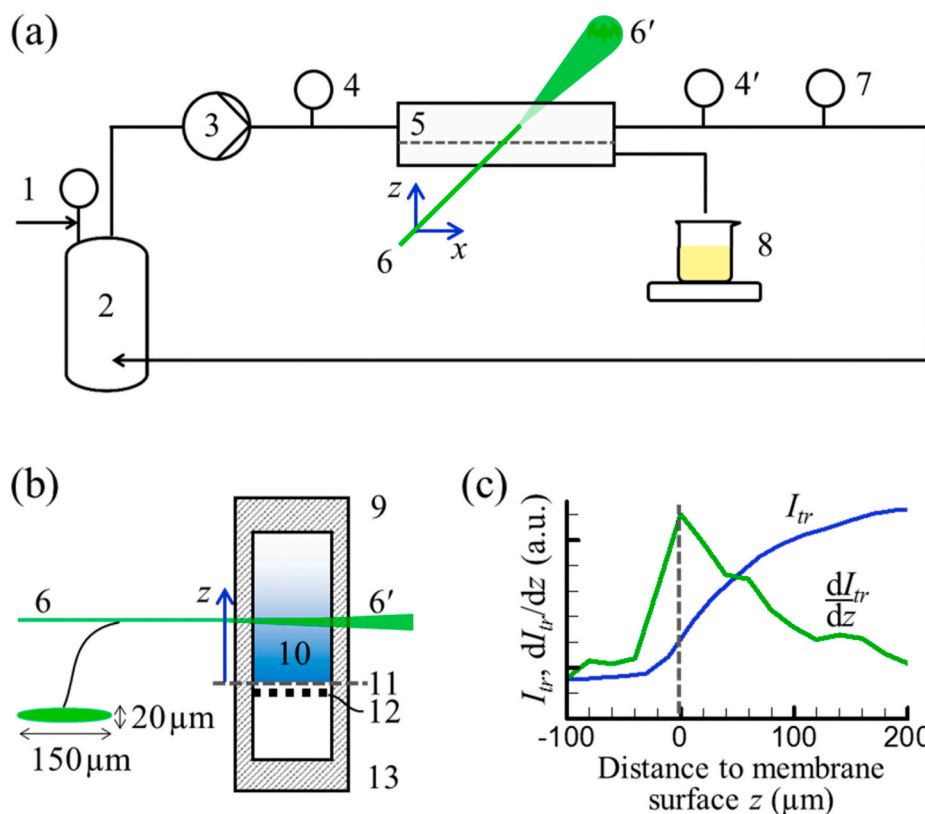


Fig. 1. (a) SAXS-filtration rig: 1 – compressed air, 2 – pressurized and thermostated vessel containing suspension, 3 – positive displacement pump, 4 and 4' – pressure gauges, 5 – crossflow SAXS-filtration cell, 6 and 6' – incident and scattered X-ray beams, 7 – magnetic flowmeter, 8 – filtrate and electronic balances; (b) transverse view of the SAXS-filtration cell: 9 – retentate part of the cell, 10 – fouling layer, 11 – membrane, 12 – membrane support, 13 – filtrate part of the cell; (c) determination of membrane surface position (dashed line) from the dependency of X-ray intensity transmitted through the cell filled with UF permeate on distance to the membrane $I_{tr}(z)$ and its derivative dI_{tr}/dz .

Table 1
Steps of the SAXS-filtration experiment.

Stage	Applied pressure ΔP (bar)	Average crossflow velocity, u_{av} ($\text{cm} \cdot \text{s}^{-1}$)	Stage duration, t (min)
Filtration	0.5 or 1.1	3.1	150
Pressure relaxation	0.1	3.1	45
Erosion	0.1	15.6	15

of the filter cell), and 2D SAXS patterns measured at different vertical positions of the filter cell (i.e. at different distances from membrane surface z) were recorded on the 2D detector EigerX4M. For a given z , the registered scattered beam intensity $I(q = 1 \text{ nm}^{-1})$ was recomputed into local casein concentration $c(z)$ using preliminarily obtained calibration curve $c = c(I(q))$ (the method is detailed in Supplementary data).

For a given SAXS-filtration experiment time t , local external membrane fouling was characterized using.

- local casein concentration distribution $c(z)$,
- excess weight of casein in the fouling layer m_f and in the gel layer m_g , which were determined by integrating excess casein concentration over the thickness of the fouling layer

$$m_f = \int_0^{z(c=c_0)} (c(z) - c_0) dz \quad (1)$$

and over the thickness of the gel layer h_g

$$m_g = \int_0^{h_g} (c(z) - c_0) dz \quad (2)$$

respectively, and.

- gel thickness h_g , which was estimated as

$$h_g = z(c = c_{sg}) \quad (3)$$

where c_{sg} is casein concentration at the point of sol-gel transition. The value of c_{sg} was estimated from the literature data: temperature-independent volume fraction of casein micelle dispersions in sol-gel transition $\phi_{sg} = 0.71$ (obtained by Doudiès et al. [43] by rheometry and osmometry of casein micelle suspensions and concentrated dispersions) and temperature-dependent casein micelle voluminosity $v = 3.9 \text{ ml} \cdot \text{g}^{-1}$ at 25°C (obtained by Nobel et al. [44] by rheometry of liquid casein micelle suspensions). The equation

$$c_{sg} = v^{-1} \phi_{sg} \quad (4)$$

then gave the value $c_{sg} = 182 \text{ g} \cdot \text{l}^{-1}$. According to experimental data obtained by Ref. [43] and literature data reviewed in the same study, the uncertainty in the determination of c_{sg} is equal to $\pm 3.5 \text{ g/l}$.

2.4. Analysis of average membrane fouling

Average membrane fouling was acquired from the data on permeate flux, which was measured using precision balances (PB 303-S, Mettler Toledo, accurate to 1 mg) in a separate series of experiments with the same rig, material and conditions as used for *in situ* SAXS-filtration. The measurements were performed at three consecutive steps:

- rate of UF permeate filtration across the clean membrane was measured at a pressure of 1.1 bar, and the hydraulic resistance of clean membrane R_{m0} was calculated;
- UF permeate was replaced with casein micelle suspension, and filtration was commenced at the same operating conditions as applied at the first step of *in situ* SAXS-filtration (Table 1); once steady-state was reached, average filtrate flux $J_{L,ss}$ was measured and the average fouled membrane resistance R_f was calculated;

(iii) retentate was replaced with UF permeate and transmembrane pressure was reduced to zero for 20 min (while keeping the same average crossflow velocity $u_{av} = 3.1 \text{ cm} \cdot \text{s}^{-1}$) in order to rinse the membrane and remove the labile part of the fouling layer; transmembrane pressure was then increased to 1.1 bar, the rate of UF permeate filtration across the rinsed membrane was measured, and the average membrane resistance with remaining (residual) fouling R_r was calculated.

These experiments were repeated in duplicate. Average R_m , R_f and R_r values (all calculated using Darcy's equation using the filtrate viscosity $\mu_f = 0.89 \text{ mPa} \cdot \text{s}$) are presented as experimental points, and (min – max) intervals are presented as error bars.

2.5. Modeling of steady-state filtration and relaxation to analyze the reversibility of deposit formation

A model was developed to describe the distribution of external membrane fouling at the steady-state stage of crossflow filtration of the casein micelle suspension (see Annex A).

Methods were developed to determine the compressibility–permeability of the deposit and to analyze the reversibility of deposit compression using filtration and pressure relaxation data (see Annex B).

3. Results and discussion

3.1. General results on membrane fouling

Fig. 2 gives average filtrate flux J_L obtained during crossflow filtration of casein micelle dispersions at $\Delta P = 0.5 \text{ bar}$ and 1.1 bar .

Fig. 2 shows that at both studied pressures, (i) the steady state was attained after about 60–80 min of filtration (as soon as J_L leveled off) and (ii) filtration operated at limiting flux conditions (as soon as the average steady-state flux became independent of ΔP).

Average intensity of membrane fouling at different transmembrane pressures was evaluated from the average hydraulic membrane resistance values measured at different steps of the experiment (presented in Table 2).

Table 2 shows that filtration at both ΔP levels resulted in severe membrane fouling: $R_f > R_{m0}$. As soon as the limiting flux was attained at

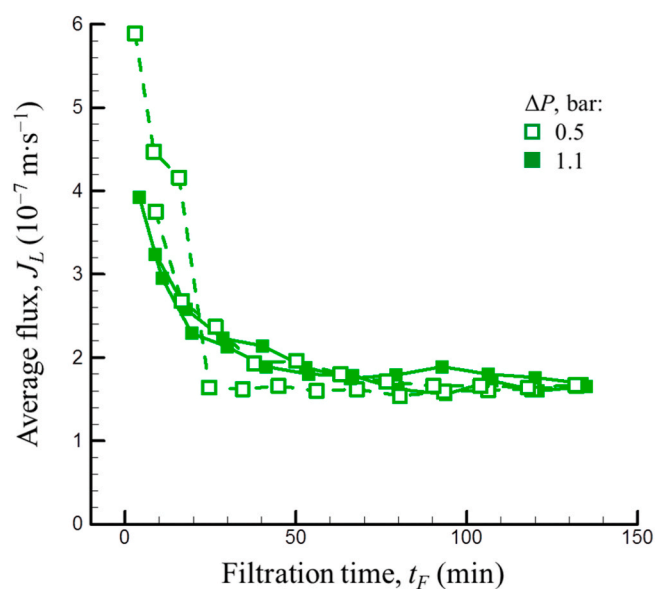


Fig. 2. Filtrate flux plotted against filtration time at constant applied pressure $\Delta P = 0.5 \text{ bar}$ (open symbols, dashed lines) and 1.1 bar (solid symbols, solid lines). Two filtration experiments were done at each ΔP .

both ΔP , this is explained by a low average crossflow velocity $u_{av} = 3.1 \text{ cm} \cdot \text{s}^{-1}$ that led to the formation of a thick deposit. Rinsing the membrane removed a majority of the fouling: $R_r \ll R_f$. This suggests that the membrane fouling by the deposit was at least partially reversible. However, residual fouling was an order of magnitude higher than the hydraulic resistance of clean membrane, and was higher in the experiment with the higher applied pressure, which is qualitatively consistent with the theory of particle aggregation at the membrane surface [17,20,21,29]: a higher applied pressure results in a thicker deposit and a thicker irreversibly-aggregated fraction of deposit attached to the membrane. We carried out SAXS analysis on the fouling layer to verify this hypothesis and to distinguish the reversible and irreversible parts of the deposit.

3.2. Casein accumulation in the fouling layer

Fig. 3 charts the variation in local concentration distribution at the membrane surface during the filtration step at $\Delta P = 0.5 \text{ bar}$ (Fig. 3a) and following the relaxation and deposit erosion steps (Fig. 3b) determined via *in situ* SAXS analysis. $\Delta P = 1.1 \text{ bar}$ at the filtration step gave very similar data, which is reported in Supplementary data, Fig. S1.

According to Fig. 3a, the deposit (gel with $c > c_{sg}$) appeared at the membrane surface at $t_F < 10 \text{ min}$, and the following filtration resulted in deposit growth and increasing concentration (deposit formation had previously been observed, for example in Ref. [37], during the ultrafiltration of anisotropic nanocolloids). The $c(z)$ curves practically merged at $t_F \geq 130 \text{ min}$, which implies that the local steady state in the middle of the filter channel ($x = 5 \text{ cm}$) was attained at this time (e.g. as in Ref. [36], where the steady-state structure of the fouling layer is observed at the steady-state stage of crossflow ultrafiltration of Laponite). This time was longer than the time required for average filtrate flux to stabilize, $t_F = 60\text{--}80 \text{ min}$ (according to Fig. 2), which probably reflects a higher sensitivity of local SAXS analysis to changes in filtration kinetics than to average flux measurement.

After the pressure decrease to $\Delta P = 0.1 \text{ bar}$ at the relaxation step (Fig. 3b), local casein concentration in the deposit progressively decreased at every distance from the membrane, this confirming casein micelle deposits can swell after pressure relaxation [17] (according to Fig. S1b, the same is true for the gel obtained at $\Delta P = 1.1 \text{ bar}$). Moreover, Fig. 4 and S2 suggest that deposit weight and thickness both decreased after the drop in pressure. Deposit swelling was therefore assisted by redispersion of the casein micelles (at least from the external and initially less-concentrated part).

Note that at both studied pressures m_b , m_g and h_g increased abruptly when the filtration pressure relaxed (Fig. 4a,b and S2). This can be explained by an instant shift of the flexible polymeric filtration membrane away from the rigid membrane support due to the instant reduction of TMP [39,40,62] (although a low TMP of 10 kPa was maintained in order to reduce this effect during the pressure relaxation). The shift of the membrane towards positive z brought the inner sublayer of casein micelles, which was localized close to the membrane surface ($z < 20 \mu\text{m}$) and was not accounted for in the calculations of m_b , m_g and h_g during the earlier filtration step, into the scope of SAXS analysis ($z > 20 \mu\text{m}$) [39,40,62], resulting in an apparent increase of m_b , m_g and h_g . According to Fig. 4b, the membrane shifted for $15\text{--}17 \mu\text{m}$ (same as in

Table 2

Average hydraulic resistance values in experiments with $\Delta P = 0.5 \text{ bar}$ and 1.1 bar (applied during deposit formation).

Pressure applied at filtration step, ΔP (bar)	Hydraulic resistance of clean membrane R_{m0} (10^{13} m^{-1})	Hydraulic resistance of fouled membrane at steady-state, R_f (10^{13} m^{-1})	Hydraulic resistance of rinsed membrane, R_r (10^{13} m^{-1})
0.5	0.5 ± 0.1	33 ± 3	4.9 ± 1.3
1.1	0.5 ± 0.1	74 ± 7	8.0 ± 0.3

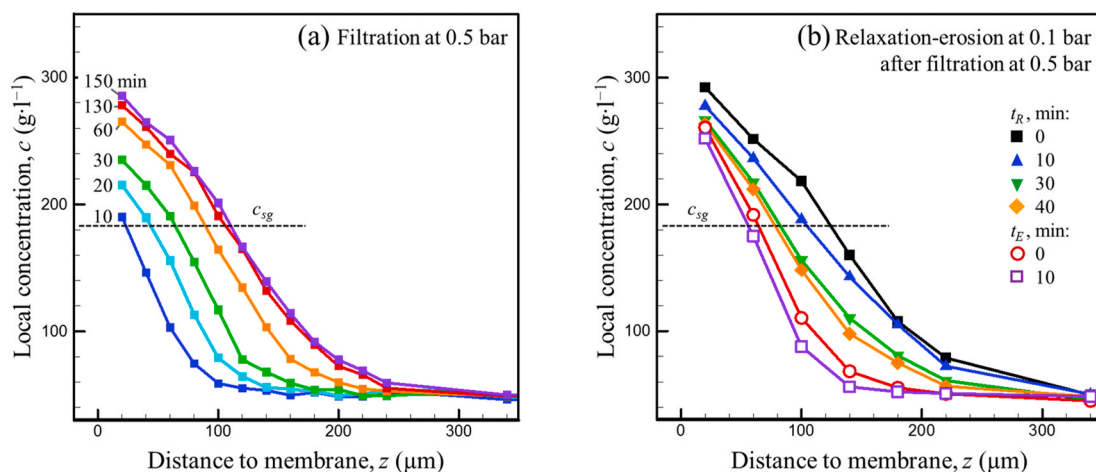


Fig. 3. Casein concentration c plotted against distance to membrane z during (a) filtration of casein micelle dispersions at $\Delta P = 0.5$ bar (average crossflow velocity $u_{av} = 3.1 \text{ cm} \cdot \text{s}^{-1}$) and (b) following relaxation ($\Delta P = 0.1$ bar, $u_{av} = 3.1 \text{ cm} \cdot \text{s}^{-1}$) and erosion ($\Delta P = 0.1$ bar, $u_{av} = 15.6 \text{ cm} \cdot \text{s}^{-1}$) determined via *in situ* SAXS analysis. Times of filtration t_F , relaxation t_R , and erosion t_E are shown at the head of the curves (in minutes). The dashed line charts the sol-gel transition concentration c_{sg} determined via Eq. (4).

Ref. [62]), which was small compared to the lowest measured gel thickness. Because of this membrane shift, $c(z)$ profiles measured at $t_R = 0$ min are slightly higher as compared to the last profiles measured during the filtration stage (Fig. 3a and S1a vs. Fig. 3b and S1b).

The decrease of m_g and h_g at $x = 5$ cm (Fig. 4 and S2) during pressure relaxation is qualitatively consistent with the decrease of average fouled membrane resistance after membrane rinsing (Table 2) but the decrease of average fouled membrane resistance was quantitatively more significant: in experiments with filtration pressure $\Delta P = 1.1$ bar for example, $m_g(t_F = 150 \text{ min})/m_g(t_R = 20 \text{ min}) \approx 1.4$ whereas $R_f/R_r \approx 9.3$. We explain this by the distribution of the deposit thickness over the membrane length, as it follows from Eq. (A6) and (A14) (Annex A) (and other models of crossflow filtration with deposit formation [22,45]) that deposit thickness increases with x (note that TMP was near constant along the filter channel). Note too that the increase of the fouling layer thickness with x was previously observed by *in situ* SAXS-crossflow filtration of skim milk [34,35] (also for the case of near constant TMP). As soon as deposit swelling rate is inverse to h_g^2 [46,47], deposit removal after the pressure relaxation (and the corresponding decrease of the local fouled membrane resistance) can be faster at lower x . This can result in the larger decrease of average membrane fouling (estimated

from R_f and R_r) compared to local fouling in the middle of the filter channel (estimated by m_g or h_g). This result confirms the idea that average hydraulic resistance of rinsed membrane R_r is insufficient for firm characterization of residual membrane fouling [48].

According to Fig. 4 and S2, dependencies $m_g(t)$ and $h_g(t)$ did not level off during relaxation. At the beginning of erosion, $m_g(t)$ and $h_g(t)$ decreased steeply, which can be explained by removal of a loose swelled part of the gel after the five-fold increase in wall shear stress (Table S2). $m_g(t)$ and $h_g(t)$ then continued to gradually decrease. Therefore, the data presented in Fig. 4 and S2 is insufficient to firmly evidence deposit irreversibility, and so a comprehensive analysis of swelling kinetics is required.

3.3. Analysis of deposit compressibility-permeability

The analysis of deposit compressibility-permeability is based on applying the model of steady-state crossflow filtration with deposit formation (model described in Annex A) to the data obtained at the steady-state stage of SAXS-filtration. Fig. 5 compares concentration distribution profiles in the fouling layer $c(z)$ obtained at $\Delta P = 0.5$ bar ($t_F \geq 130$ min) and 1.1 bar ($t_F \geq 105$ min) when steady-state was reached (i.

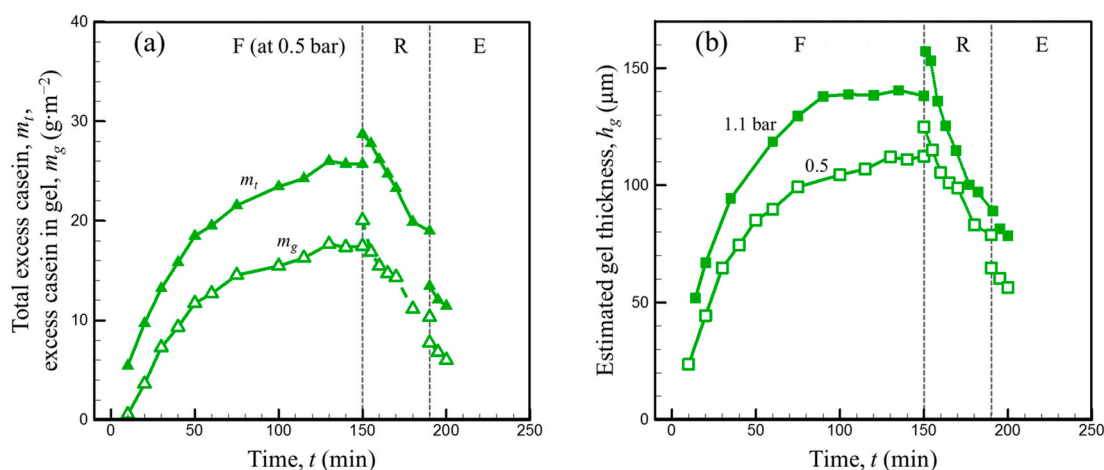


Fig. 4. (a) Total excess quantity of casein at the membrane surface m_t (solid symbols) and that in the deposit (gel layer) m_g (open symbols) at different steps of the experiment with filtration pressure $\Delta P = 0.5$ bar; (b) time-course of deposit (gel) thickness h_g in experiments with $\Delta P = 0.5$ bar (open symbols) and 1.1 bar (solid symbols). Dashed verticals correspond to the transitions between filtration (F), relaxation (R), and erosion (E) steps that mark changes in pressure or average crossflow velocity.

e. m_g and J_L are constant).

The deposit obtained at higher ΔP was more concentrated due to higher compression of casein micelles [17,18]. Filtration at higher pressure increased local gel thickness h_g by 1.2 (Fig. 5), while the average resistance of fouled membrane at steady state increased by 2 (Table 2), which is explained by significantly decreasing permeability of casein micelles gel with compression [17,29]. At the steady state, the concentration distribution on the CP layer (i.e. $c(z)$ in the part with $c < c_{sg}$) was practically unaffected by ΔP value (Inset in Fig. 5) because as it evolved at the same filtrate flux and shear stress conditions at both ΔP .

At both studied pressures, as soon as filtration was at limiting flux conditions, we analyzed the SAXS-filtration data as follows and determined deposit compressibility-permeability using Eqs. (B1) and (B2) (Annex B). Average steady-state flux $J_L = 1.7 \pm 0.1$ ($10^{-7} \text{ m} \cdot \text{s}^{-1}$) (Fig. 2) was used to calculate local filtrate flux at $x = 5 \text{ cm}$ (where $c(z)$ profiles were measured). Despite the difference in $J(0)$ values (calculated from the hydraulic resistance of clean membrane $R_{m0} = 5 \cdot 10^{12} \text{ m}^{-1}$), i.e. $J(0) = 1.4 \cdot 10^{-5} \text{ m} \cdot \text{s}^{-1}$ at $\Delta P = 0.5 \text{ bar}$ and $3.1 \cdot 10^{-5} \text{ m} \cdot \text{s}^{-1}$ at $\Delta P = 1.1 \text{ bar}$, the two different pressures gave practically the same $M(c_{sg}, \tau_w) = 7.3 \cdot 10^{-27} \text{ Pa}^3 \text{ m}^2 \cdot \text{s}$ and $J(x = 5 \text{ cm}) = 1.4 \cdot 10^{-7} \text{ m} \cdot \text{s}^{-1}$, as expected for filtration in limiting flux conditions with the formation of relatively permeable CP layer and significantly less permeable gel. The obtained value of $J(x = 5 \text{ cm})$ was used to calculate the function $kd\pi/dc$ (complex material property) from the steady-state $c(z)$ profiles (Fig. 5) via Eq. (B3) (Annex B). Fig. 6 presents the $(kd\pi/dc)^{-1}$ obtained through this method of SAXS-filtration data analysis.

The $kd\pi/dc$ values obtained (symbols) were compared with the dependency reported by Bouchoux et al. [29] via a series of experiments on osmotic compression (to determine the dependency of $d\pi/dc$ on c) and dead-end filtration (to determine the dependency of k on c). Despite the distinct difference in $c(z)$ profiles obtained at different filtration pressures (Fig. 5), dependencies of $(kd\pi/dc)^{-1}$ on c calculated from these profiles practically coincide (symbols in Fig. 6), as expected for a material property. It is reasonable to speculate that the bell-like shape of the

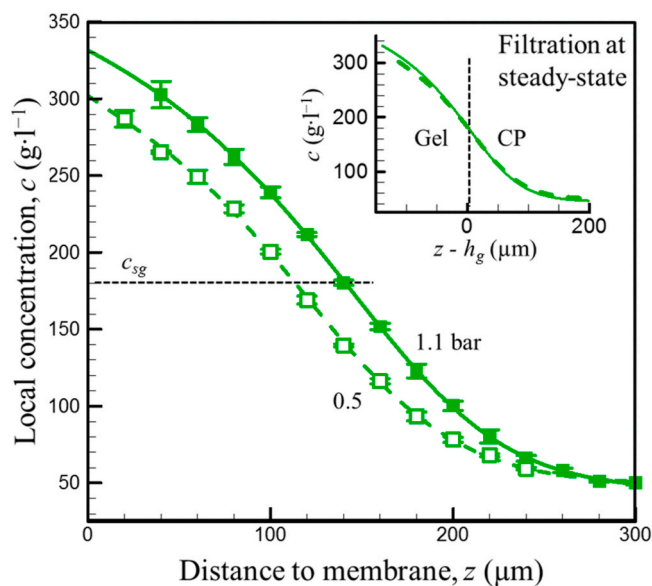


Fig. 5. Steady-state $c(z)$ profiles measured in SAXS-filtration experiments at different ΔP . The open symbols and dashed curve plot filtration at 0.5 bar (points are average values from three $c(z)$ profiles obtained at $t_F = 130$ –150 min); solid symbols and solid curve plot filtration at 1.1 bar (points are average values from four $c(z)$ profiles obtained at $t_F = 105$ –150 min). Error bars present standard deviations, curves correspond to least-squares fitting of SAXS-filtration data using proper polynomial equations. The dotted horizontal corresponds to the sol-gel transition concentration c_{sg} obtained from Eq. (4). Inset: the same curves merged at point $[z = h_g, c = c_{sg}]$ (i.e. at the sol-gel border, materialized by a dashed vertical).

obtained dependency $1/(kd\pi/dc)$ on c is related to the dominance of permeability factor (k decreases as c increases) over compressibility factor ($d\pi/dc$ increases as c increases) at $c < c_{sg}$, and vice versa. The curves obtained here pass through a maximum at $c \approx c_{sg} = 182 \text{ g} \cdot \text{l}^{-1}$ (value deduced by Nöbel et al. [44] from independent rheological measurements). This connects to the expected significant change in material properties in the point of sol-gel transition [22,29] that indirectly supports the validity of the current analysis.

Note that $kd\pi/dc$ values obtained at low c (corresponding to the outer part of the CP layer) may be overestimated due to the constant $J(x = 5 \text{ cm}) \neq f(z)$ used in the calculations. Constant $J(x) \neq f(z)$ is equivalent to the generally applied assumption about the constancy of solid-liquid velocity in the CP layer (assumptions (11) and (12) in Annex A), and does not therefore account for solid movement towards the membrane, which is greater at lower solids concentration in the CP layer [49]. However, further analysis demonstrated that this factor had no significant influence on our conclusions concerning the reversibility of gel compression.

Interestingly, the values found here via analysis of SAXS-crossflow-filtration data for microscopic objects (deposit layers) (symbols in Fig. 6, fairly fast gel formation, $t \approx 2 \text{ h}$, and steady-state filtration) were of the same order of magnitude as the values found by Bouchoux et al. [29] via osmotic compression (fairly slow gel formation, $t \approx 10$ –100 h) and dead-end filtration (unsteady) for macroscopic gel samples. However, the difference in curve behavior (data from Bouchoux [29] versus here) is unclear and requires additional research.

3.4. Modeling and analysis of deposit swelling, evidence for irreversibility of deposit compression

Modeled and experimentally observed gel swelling kinetics can be compared in order to confirm or discard the assumption that the gel properties ($kd\pi/dc$ at given c) are independent of compression history. i. e. elucidate whether the compression of casein micelle gel obtained during crossflow filtration at different conditions is reversible, irreversible, or partially irreversible, in the filtration conditions under

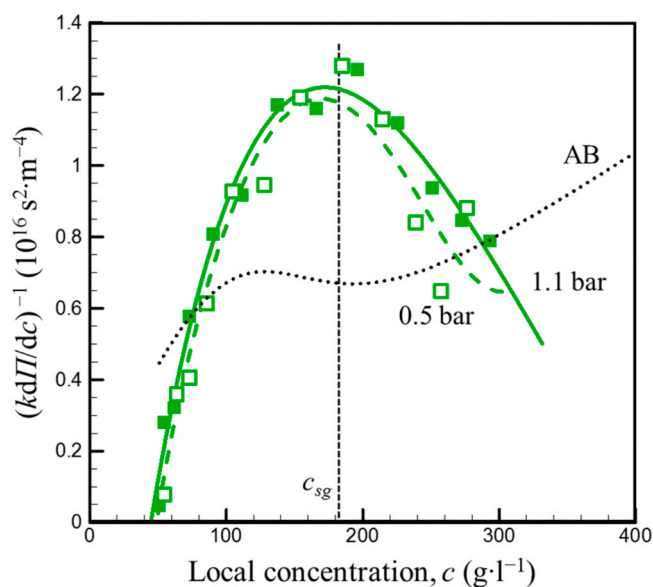


Fig. 6. Values of $(kd\pi/dc)^{-1}$ obtained at $\Delta P = 0.5 \text{ bar}$ (open symbols, dashed curve) and $\Delta P = 1.1 \text{ bar}$ (filled symbols, solid curve) from $c(z)$ profiles presented in Fig. 5. The curves plot the fitting curves presented in Fig. 5 after treatment with Eq. (B3). Dotted curve AB is calculated from the data given in Bouchoux et al. [29] that was obtained from osmotic compression and dead-end filtration experiments. The dashed vertical corresponds to the sol-gel transition concentration c_{sg} determined via Eq. (4) from rheological experiments.

study.

Since deposit swelling and redispersion was observed during the SAXS-assisted relaxation and erosion steps (Fig. 3b and S1b) and there were no evidences of completely irreversible fouling in the data presented in Fig. 4 and S2, the hypothesis on the complete reversibility of deposit compression and formation was verified. Deposit swelling after the pressure decrease from 0.5 bar to 0.1 bar was modeled using Eqs. (B4), (B6) – (B8) and (B9) (presented in Annex B). The properties of the swelling deposit (with the same initial $c(z)$ distribution as that determined via SAXS, Fig. 3b) were described using the dependency of $k d \Pi / d c$ on c obtained for compressed deposit from the data on steady-state filtration (Fig. 6) and dependency $\Pi(c)$ obtained by Doudiès et al. [43] from osmotic compression experiments (presented in Supplementary data). We therefore assumed that deposit compression was completely reversible. Two different mechanisms of deposit swelling were considered (since neither had previously been experimentally confirmed): without and with filtrate absorption across the membrane (illustrated in Annex B, Figs. B1a and B1b, respectively). The $c(z)$ curves obtained by modelling with the same relaxation times t_R as in the SAXS–relaxation experiment with pressure reduced from $\Delta P = 0.5$ bar–0.1 bar (Fig. 3b) are presented in Fig. 7. The corresponding modeling results for the deposit obtained at 1.1 bar are presented in Supplementary data, Fig. S3.

Regardless of the assumed swelling conditions (i.e. no crossflow and high fouled membrane resistance, which, as discussed in the part B3 of Annex B, can only underestimate the swelling rate; the result of calculations with $R_m = 4.9 \cdot 10^{12}$, which is the hydraulic resistance of clean membrane, was not essentially different from that presented in Fig. 7b), modeling predicts significantly faster gel swelling compared to experimental data. Roughly, the actual swelling (Fig. 3b) was more than 10 times slower than modeled swelling (Fig. 7). The same discrepancy between the modeled and experimental swelling kinetics was obtained for the gel formed at 1.1 bar (Figs. S1 and S3 in Supplementary data). This conclusion holds for both assumed filtrate uptake mechanisms (with and without filtrate uptake across the membrane). In the current study, the more than tenfold deviation between modeled and experimental data cannot be explained by any reasonable experimental error (which would require a more than tenfold erroneous underestimation of local flux and $k(c) d \Pi(c) / d c$ here and in Bouchoux et al. [29], Fig. 6) or more than threefold underestimation of gel thickness [47]) (model results, not shown).

A more reasonable explanation for the observed slow swelling kinetics is a significant difference in assumed and actual deposit properties, i.e. partial irreversibility of gel formation and compression. It is

reasonable to suggest that filtration–compression of casein micelle gel is described by different $k(c) d \Pi(c) / d c$ dependencies under conditions of local pressure increase (filtration, deposit formation) and decrease (relaxation, gel swelling). The filtration scholarship usually explains this using the framework of DLVO theory applied to the case of a filter cake on a membrane surface: irreversible particle aggregation occurs when the fouling layer reaches and exceeds the critical sol–gel transition concentration [17,20–22], resulting in decreased particles repulsion, significant lowering of $\Pi(c)$ (and a corresponding lowering of $d \Pi(c) / d c$ [22,26–28,50–52]), and a slowdown of osmotic-process filtrate uptake.

Interestingly, contrary to the simple case of DLVO theory, in the case of casein micelles, particle repulsion forces ultimately exceeded the attraction forces (at least in the external, less concentrated part of the deposit), since the deposit swelled and redispersed. Also note that swelling and redispersion of casein micelle gels obtained by osmotic compression was observed in swelling experiments even without applied shear [18]. This demonstrates the conventionality of the term “irreversibility” in the discussion of compression of deposits and dispersions of casein micelles (and soft/elastic aggregating colloids in general).

Rigorous characterization of the reversibility of casein micelle deposits (i.e. determination of $k(c, t_R) d \Pi(c, t_R) / d c$ in the course of pressure relaxation) can be done by analyzing the $c(z, t_R)$ curves (i.e. as presented in Fig. 3b and S1b) by the Matano method, for instance. However, it requires knowledge of the local filtrate flux $J(x)$, which is difficult to measure, when the deposit with changing thickness $h_g(x)$ is obtained in a crossflow filtration experiment. This can be accomplished in *in situ* SAXS experiments on dead-end filtration–relaxation, and would also clarify the possible influence of time on $\Pi(c)$ dependency in the compression and swelling of filtration deposits.

4. Conclusions

Crossflow ultrafiltration of casein micelle dispersions was studied using a special-purpose SAXS–filtration cell. Filtration experiments comprised three consecutive stages: deposit formation at constant applied pressure (0.5 bar or 1.1 bar) and crossflow velocity ($3.1 \text{ cm} \cdot \text{s}^{-1}$), deposit relaxation after relaxing filtration pressure down to 0.1 bar at the same constant crossflow velocity ($3.1 \text{ cm} \cdot \text{s}^{-1}$), and deposit erosion at increased crossflow velocity ($15.6 \text{ cm} \cdot \text{s}^{-1}$). The time–course of deposit formation, relaxation and erosion was observed via *in situ* SAXS which enabled the measurement of local casein micelles concentration profiles at the membrane surface (i.e. in the deposit and the concentration polarization layer) with a spatial resolution of $20 \text{ } \mu\text{m}$ at different

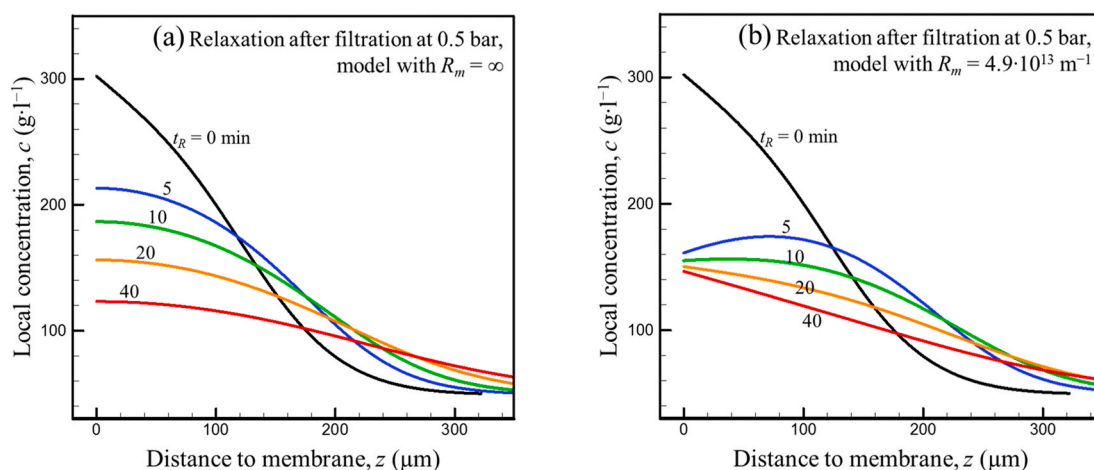


Fig. 7. Model results for $c(z)$ concentration distribution profiles during swelling at $\Delta P = 0.1$ bar after filtration at $\Delta P = 0.5$ bar: (a) without filtrate flow across the membrane; (b) with filtrate flow and uptake across the membrane with $R_m = 4.9 \cdot 10^{13} \text{ m}^{-1}$. Relaxation time t_R is shown near the curves (in min). Initial $c(z)$ was taken from experimental data (Fig. 5). The $k d \Pi / d c$ and $\Pi(c)$ dependencies required for modeling were taken from our SAXS–filtration data (Fig. 6) and from osmotic stress experiments (Doudiès et al. [43]), respectively.

experiment timepoints. Local membrane fouling by the deposit was quantified via the deposit thickness and casein quantity accumulated in the deposit. In addition, average membrane fouling was quantified via average resistances of fouled and rinsed membranes. Data analysis focused on characterization of the reversibility of deposit-driven membrane fouling.

It was concluded that membrane fouling by casein micelle deposits is at least partially reversible at both studied filtration pressures: i.e. (i) local deposit concentration decreased after the pressure release at every distance from the membrane (the deposit swelled), and (ii) the pressure relaxation and following erosion reduced the quantity of deposit as well as the average resistance of the fouled membrane (the deposit partially redispersed). However, the local deposit quantity decreased less than the average fouling resistance, which is explained by the distribution of deposit thickness along the filter channel. It was thus confirmed that measuring average hydraulic resistance (of clean, fouled and rinsed membrane) is less informative for the membrane fouling characterization than direct fouling analysis.

The dependency of deposit compressibility–permeability on its local concentration (which is a complex material property of the deposit) was obtained from casein concentration distribution and average filtrate flux measured at the steady-state of filtration using the developed model of crossflow filtration of colloidal suspensions accounting for non-Newtonian rheological properties of the concentration polarization layer and deposit compressibility. The concentration dependency of compressibility–permeability obtained for the compressed deposit was used to model the kinetics of deposit swelling (under the assumption of completely reversible deposit compression). We found a large discrepancy between modeled (fast) and experimental (slow) swelling rates, prompting us to conclude that the compression of casein micelle deposits is partially irreversible, probably due to the lower osmotic

pressure in the swelling deposit compared to the compressed deposit at constant local casein concentration. This irreversibility can be explained by an aggregation of casein micelles during compression. A method for determining the local compressibility of the deposit in the course of swelling (and, thus, quantitative characterization of the reversibility of the deposit compression) is proposed.

Declaration of competing interest

The authors declare that they have no known competing financial interests or personal relationships that could have appeared to influence the work reported in this paper

Acknowledgments

The authors from STLO and LRP thank the SOLEIL Synchrotron for providing synchrotron beam time. The authors thank the French National Research Institute for Agriculture, Food and Environment (INRAE) and Brittany Regional Council for providing valuable financial support. ML thanks the INRAE's TRANSFORM department for the financial support provided for his work under the ANS project 'Emomil: étude et modélisation de la microfiltration du lait' as well as Rennes Metropole for awarding his project an 'Allocation d'installation scientifique' grant in 2019. We thank Glen McGulley for invaluable help preparing the manuscript.

LRP is part of PolyNat Carnot Institute ('Investissements d'Avenir'-grant agreement #ANR-11-CARN-030-01), Labex TEC 21 ('Investissements d'Avenir'-grant agreement #ANR-11-LABX-0030) and Glyco@Alps ('Investissements d'Avenir'-grant agreement #ANR-15-IDEX-02).

Appendix A. Supplementary data

Supplementary data to this article can be found online at <https://doi.org/10.1016/j.memsci.2021.119289>.

Annex A. Model of steady-state crossflow filtration

The model describes steady-state crossflow filtration of a colloidal suspension, leading to the formation of a concentration polarization (CP) layer that is optionally followed by formation of a compressible deposit (a gel having a yield stress that exceeds an applied wall shear stress). Local solid concentration c and local permeability k of the CP layer and the gel can depend on local osmotic pressure Π (in the CP layer) or local solid compressive pressure p_s (in the gel). The CP layer can exhibit concentration-dependent non-Newtonian rheological behavior, which means that $\dot{\gamma} = \dot{\gamma}(c, \tau)$, where $\dot{\gamma}$ is a shear rate and τ is a shear stress.

A1. Model derivation

The current model derivation follows a general approach used by Gaddis (1992) [45] and Bacchin et al. (2002) [22]. It extends the applicability of the Gaddis and Bacchin models to the case of a non-Newtonian CP layer.

The following assumptions, which are usual in crossflow filtration modeling, were used for the model derivation:

- (1) steady-state filtration;
- (2) fully-developed crossflow;
- (3) filtration membrane is a continuum with a constant hydraulic resistance;
- (4) the membrane is fully retentive for colloidal solids;
- (5) pore blocking and other 'pore fouling' phenomena are not considered; if they are present, then hydraulic resistance of clean membrane must be replaced by fouled membrane resistance (that does not comprise CP and gel resistance) in the following equations;
- (6) the CP layer and gel thicknesses are negligible compared to filter channel dimensions;
- (7) in the CP layer, tangential gradients of crossflow velocity and particle concentration are negligible compared to the respective normal gradients (consequence of assumption (6));
- (8) local values of material properties are unique functions of solid concentration (permeability $k(c)$ and osmotic pressure $\Pi(c)$ or compressive solid pressure $p_s(c)$); these material properties are unaffected by tangential flow; local rheological properties are defined by local concentration and local shear stress;
- (9) filtrate flux is negligible compared to crossflow flux; therefore, the filtration pressure gradient is practically constant along the filter channel;

- (10) shear stress across the CP layer is constant and equal to wall shear stress τ_w (consequence of assumption (6)); τ_w is constant along the filter channel (consequence of assumptions (2) and (9));
- (11) for a given distance from the filter cell entrance x , filtrate flux is constant across the CP layer, gel and membrane.
- (12) filtrate permeation across the CP layer can be described by Darcy's equation.

The following equations are obtained for a filtration channel with simple geometry (straight filter channel with a smooth membrane surface) (Fig. A1).

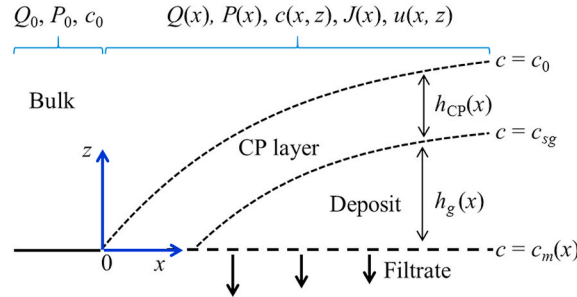


Fig. A1. Filtration of a feed suspension with colloidal solid concentration $c = c_0$ through a fully retentive membrane forms a filtrate ($c = 0$) and a CP layer of thickness $h_{CP}(x)$ and local concentration $c(x, z) > c_0$ followed by a gel (deposit) of thickness $h_g(x)$ and local concentration $c(x, z) > c_{sg}$, where c_{sg} is a sol-gel transition concentration. Local particle concentration on the membrane surface is written as $c_m(x)$.

At steady state, there is no additional particle accumulation inside the filter channel (nor particle redistribution between the flowing CP layer and the immobile gel/deposit). The total flux of particles across a transverse section of the filter channel at any distance from entrance x is equal to the total particle flux at the entrance to the filter channel $Q_0 c_0 / \rho_s$, where Q_0 is average tangential flow velocity at the entrance to the filter channel (at $x = 0$), c_0 is solid concentration in the feed suspension, and ρ_s is solid density.

Filtration results in a gradual concentration of particles in the CP layer, where $c(x, z) > c_0$. Following the idea of Gaddis [45] and Bacchin [22], the total particle flux across a transverse section of the filter channel at any distance from the entrance x is presented as a sum of two virtual components: (1) tangential transport of excess particles in the flowing CP layer, and (2) transport of suspension having the initial particle volume fraction c_0 . Therefore, the total transport of particles through any cross-section of the filter channel can be written as

$$Q_0 c_0 = a \int_{h_g(x)}^{h_{CP}(x)+h_g(x)} u(x, z) (c(x, z) - c_0) dz + Q(x) c_0 \quad (A1)$$

where $u(x, z)$ is the local tangential flow velocity of liquid and particles, $Q(x)$ is the average tangential flow velocity through the entire cross-section of the channel (including the CP layer), and a is a length of the membrane part of the perimeter of a cross-section of the filter channel (e.g. $a = 2\pi R$ in the case of cylindrical filter channel and $a = 4$ mm in the case of the present SAXS-filtration experiments with rectangular filter channel). The integration in Eq. (A1) is done over the local CP layer thickness $h_{CP}(x)$, and the lower integration limit $h_g(x)$ is the local gel thickness ($h_g(x) = 0$, if the gel is absent at a given x).

Using the definition of shear rate $\dot{\gamma}$, local tangential flow velocity $u(x, z)$ can be presented as

$$u(x, z) = \int_{h_g(x)}^z \dot{\gamma}(x, z) dz \quad (A2)$$

where $\dot{\gamma}(x, z)$ is the normal component of local shear rate (according to assumption (7), its tangential component is neglected). It is assumed that there is no slip at the CP-solid (membrane or gel) boundary.

Further description of particle transport in the CP layer requires knowledge of its local rheological properties (i.e. shear stress dependency of shear rate at a given particle concentration). In accordance with model assumptions (8) and (10), in the CP layer

$$\dot{\gamma} = \dot{\gamma}(c, \tau_w) \quad (A3)$$

Therefore, to model the filtration, we need to determine the local rheological properties in this layer (defined via Eq. (A3)) for a single value of τ_w . For a given value of τ_w , known (either modeled or experimentally-measured) dependency $\dot{\gamma}(c, \tau_w)$ can be introduced into Eq. (A2)

$$u(x, z) = \int_{h_g(x)}^z \dot{\gamma}(c, \tau_w) dz \quad (A4)$$

where $c = c(x, z)$ is unknown.

An extension of the usual assumption of conventional filtration theory (assumption (11)) for the case of crossflow filtration with CP layer formation makes it possible to apply Darcy's equation in order to relate local filtrate flux with local filtration properties of the CP layer and gel:

$$\mu_f J(x) = -k(x, z) \frac{d\Pi(x, z)}{dz} \quad (A5)$$

where μ_f is filtrate viscosity, $k(x, z)$ is local hydraulic permeability and $\Pi(x, z)$ is local osmotic pressure in the CP layer (or solid pressure in the gel, as discussed in Ref. [47]). Eq. (A5) is applied to describe the gel (immobile) and CP layer (flowing): in the current model, the usual presentation of filtrate percolation across the CP layer as a back-diffusion of particles [22,45] is replaced by Darcy's equation using osmotic pressure instead of compressive solid pressure.

In accordance with assumption (8), Eq. (A5) can be rewritten as.

$$\mu_f J(x) = -k(c) \frac{\partial \Pi(c)}{\partial c} \frac{dc}{dz} \quad (\text{A6})$$

where $c = c(x, z)$ is unknown.

The following model derivation is equivalent to that done by Bacchin et al. (2002). Expression of dz from Eq. (A6)

$$dz = -\frac{k(c)}{\mu_f J(x)} \frac{\partial \Pi(c)}{\partial c} dc \quad (\text{A7})$$

with its following substitution into Eq. (A4) yields

$$u(x, z) = -\frac{1}{\mu_f J(x)} \int_{h_g(x)}^z \dot{\gamma}(c, \tau_w) k(c) \frac{\partial \Pi(c)}{\partial c} dc \quad (\text{A8})$$

Substitution of Eq. (A7) and (A8) into Eq. (A1) yields

$$Q_0 c_0 = \frac{a}{\mu_f^2 J(x)^2} \int_{h_g(x)}^{h_g(x)+h_{CP}(x)} (c - c_0) k(c) \frac{\partial \Pi(c)}{\partial c} \left[\int_{h_g(x)}^z \dot{\gamma}(c, \tau_w) k(c) \frac{\partial \Pi(c)}{\partial c} dc \right] dc + Q(x) c_0 \quad (\text{A9})$$

The upper limit of the first integral in Eq. (A9) corresponds to the boundary between CP layer and bulk suspension, where $c = c_0$ (it is also assumed that relatively low filtrate flux has no significant influence on bulk concentration). When the gel is absent, the lower integration limit $h_g(x)$ corresponds to the membrane surface position, where $c = c_m(x)$. When the gel is present on the membrane, it corresponds to the CP layer–gel surface position, where $c = c_{sg}$. The particle concentration in the point of sol–gel transition c_{sg} does not depend on x but depends on τ_w (assumption (8)) (i.e. an element of external membrane fouling layer flows and so belongs to sol and not gel if its local particle concentration corresponds to the yield stress, which is lower than the wall shear stress τ_w). Hence, Eq. (A9) can be rewritten as

$$Q(x) = Q_0 - \frac{a}{c_0 \mu_f^2 J(x)^2} \int_{c_0}^{c_m(x)} (c - c_0) k(c) \frac{\partial \Pi(c)}{\partial c} \left[\int_c^{c_m(x)} \dot{\gamma}(c, \tau_w) k(c) \frac{\partial \Pi(c)}{\partial c} dc \right] dc \quad (\text{A10a})$$

for values of x corresponding to the membrane covered by flowing CP layer, or

$$Q(x) = Q_0 - \frac{a}{c_0 \mu_f^2 J(x)^2} \int_{c_0}^{c_{sg}} (c - c_0) k(c) \frac{\partial \Pi(c)}{\partial c} \left[\int_c^{c_{sg}} \dot{\gamma}(c, \tau_w) k(c) \frac{\partial \Pi(c)}{\partial c} dc \right] dc \quad (\text{A10b})$$

for values of x corresponding to the membrane covered by solid gel.

Also, the value of $Q(x)$ decreases with x due to filtrate formation

$$\frac{dQ(x)}{dx} = -aJ(x) \quad (\text{A11})$$

where $J(x)$ is local filtrate flux.

A2. The model solution

The current experimental SAXS–filtration data was obtained for the case of the limiting fluxes when the gel is formed at the entire surface of the membrane. Consequently, this paper only presents the part of the model that corresponds to the case described by Eq. (A10b) (i.e. when the gel is present on the membrane surface starting from $x = 0$). In this case, Eqs. (10b) and (11) are sufficient for the model solution.

For a given suspension (given value of c_0 and given dependencies $k(c)$, $\Pi(c)$ and $\dot{\gamma}(c, \tau_w)$) subjected to a given shear stress τ_w (that determines c_{sg} and $\dot{\gamma}(c, \tau_w)$), the value of the double integral in Eq. (A10b) is a constant, which depends only on c_{sg} and does not vary with x . Therefore, Eq. (A10b) can be rewritten as

$$Q(x) = Q_0 - \frac{aM(c_{sg}, \tau_w)}{c_0 \mu_f^2 J(x)^2} \quad (\text{A12})$$

where $M(c_{sg}, \tau_w)$ is the said constant

$$M(c_{sg}, \tau_w) = \int_{c_0}^{c_{sg}} (c - c_0) k(c) \frac{\partial \Pi(c)}{\partial c} \left[\int_c^{c_{sg}} \dot{\gamma}(c, \tau_w) k(c) \frac{\partial \Pi(c)}{\partial c} dc \right] dc \quad (\text{A13})$$

In the case of limiting flux discussed here, the filtrate flux distribution is described by the following solution of the system of Eq. (A11) – (A13):

$$J(x)^{-3} = J(0)^{-3} + \frac{3}{2} \frac{c_0 \mu_f^2 x}{M(c_{sg}, \tau_w)} \quad (\text{A14})$$

where $J(0)$ is the flux at $x = 0$ (as soon as the case of the limiting flux is discussed, when the gel appears at $x = 0$). This is a usual filtrate flux distribution [22,45,53]. The experimentally-measured average filtrate flux over the membrane length L , J_L , is then determined by integration of Eq. (A14) as

$$J_L = \frac{M(c_{sg}, \tau_w)}{c_0 \mu_f^2 L} \left[\left(\frac{3}{2} \frac{c_0 \mu_f^2 L}{M(c_{sg}, \tau_w)} + J(0)^{-3} \right)^{2/3} - J(0)^{-2} \right] \quad (\text{A15})$$

Eq. (A14) and (A15) were applied for the quantitative analysis of SAXS–filtration-relaxation data, as explained in Annex B.

Annex B. Quantitative analysis of SAXS–filtration-relaxation data

The model presented in Annex A can be applied in order to characterize the deposit properties, i.e. to obtain the dependency $k\partial\Pi/\partial c$ on c at the steady state of filtration. This the dependency of $k\partial\Pi/\partial c$ on c can be used to predict deposit swelling, assuming that the swelling deposit is characterized by the same dependency of $k\partial\Pi/\partial c$ on c as the compressed deposit (i.e. that deposit compression is reversible). This assumption can be verified by comparing modeled against experimental data deposit swelling kinetics. Below we detail the methods for filtration data analysis and modeling of deposit swelling kinetics that are required for this comparison.

B1. Method of SAXS–filtration data treatment

When the average filtrate flux J_L is measured at the steady-state limiting flux conditions, Eq. (A15) can be used to obtain the value of $M(c_{sg}, \tau_w)$ (other parameters of Eq. (A15) are known constants, while $J(0)$ can be equated to the filtrate flux across the clean membrane J_0):

$$J_L, J_0 \rightarrow M(c_{sg}, \tau_w) \quad (\text{B1})$$

Also, when $J_0 \gg J_L$, the value of J_0 has negligible impact on the result of this calculation.

The value of $M(c_{sg}, \tau_w)$, which is independent of x , can be used to obtain local filtrate flux $J(x)$ via Eq. (A14) for the value of x that corresponds to the position of the observation window in the SAXS–filtration-relaxation experiment ($x = 5$ cm in the current study):

$$M(c_{sg}, \tau_w), x \ \& \ J_0 \rightarrow J(x) \quad (\text{B2})$$

The $J(x)$ value thus obtained can be used together with the solid concentration gradient dc/dz , which is obtained directly from SAXS–filtration data $c(z)$, in order to obtain the dependency of $k\partial\Pi/\partial c$ on c via Eq. (A6):

$$J(x) \ \& \ c(z) \rightarrow k(c) d\Pi(c)/dc \quad (\text{B3})$$

B2. Modeling of relaxation

The function $k(c)d\Pi(c)/dc$, which can be determined from SAXS–filtration data using Eq. (B3), is an integral measure of the filterability–compressibility of the object: for example, $k(c)d\Pi(c)/dc$ is a major factor in expressions of the consolidation coefficient in conventional filtration–consolidation theory [54,55] and for solid diffusivity in compressional rheology [56,57]. According to conventional filtration theory, this dependency determines deposit kinetics in filtration as well as the kinetics of deposit relaxation. Therefore, comparison of filtration data (obtained as local pressure increases) and relaxation data (obtained as local pressure decreases) can inform on the sample's response to the applied pressure variation (e.g. on the reversibility of membrane fouling by the gel).

Modeling the gel swelling during pressure relaxation under the crossflow is a difficult task. However, we can demonstrate that simple analysis of swelling without the crossflow is sufficient to evaluate the gel reversibility here.

In the absence of crossflow, colloidal gel relaxation kinetics in presence of a CP layer can be described using a basic consolidation equation (see, for example [47], and references cited therein):

$$\frac{\partial c}{\partial t} = \frac{c^2}{\mu_f \rho_s^2} \frac{\partial}{\partial \omega} \left(c k(c) \frac{\partial \Pi(c)}{\partial c} \cdot \frac{\partial c}{\partial \omega} \right) \quad (\text{B4})$$

where t is swelling duration and ω is a material coordinate related with the distance to the membrane z as

$$d\omega = (c/\rho_s) dz \quad (\text{B5})$$

(which means that the ρ_s value is not required to determine the concentration distribution curves $c(z)$ during swelling via Eqs. (B4) and (B5)).

Eq. (B4) can be solved and concentration distribution curves $c(z,t)$ can be obtained, provided that it is coupled with proper initial and boundary conditions and that the dependency of $k\partial\Pi/\partial c$ on c is known ([47] and references cited therein). The initial condition is the initial concentration distribution (before the swelling), which is obtained from the experimental SAXS–filtration data $c(z)$ at the steady-state of filtration:

$$c = c(\omega) \quad \text{at } t = 0 \quad (\text{B6})$$

The boundary condition at the CP layer–bulk suspension interface is

$$c = c_0 \quad \text{at } \omega_0 \quad (\text{B7})$$

Two boundary conditions can be considered at the gel–membrane interface (Fig. B1).

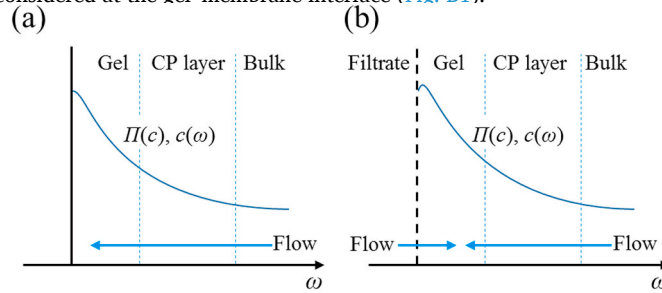


Fig. B1. Explanatory scheme for gel swelling during pressure relaxation due to liquid absorption under the osmotic pressure gradient: (a) liquid is absorbed across the polarization layer only; (b) filtrate is also absorbed across the membrane.

In the absence of filtrate flow across the membrane (neither in nor out of the filter channel, as in Fig. B1a), the condition is

$$dc/d\omega = 0 \quad \text{at } \omega \quad (\text{B8})$$

This condition can be satisfied, for example, when membrane pores are blocked by gas bubbles that appear after the pressure decrease at the pressure relaxation step of the experiment. Also, the application of Eq. (B8) neglects the small pressure that was applied to the system from the bulk side to maintain membrane position during the relaxation step.

When the membrane is permeable to filtrate flow during the relaxation (as in Fig. B1b), the boundary condition is [47].

$$\frac{dc}{d\omega} = \frac{\Pi(c) - \Delta P_R}{R_m} \frac{\rho_s}{ck(c)\partial\Pi(c)/\partial c} \quad \text{at } \omega = 0 \quad (\text{B9})$$

where ΔP_R is the pressure maintained in the filter channel during the relaxation, and R_m is membrane resistance to filtrate flow.

B3. SAXS–filtration-relaxation data analysis

The system of Eqs. (B4), (B6)–(B8) or (B9) describes swelling of a gel covered with a CP layer in the absence of crossflow (which follows from the constancy of ω_0 in Eq. (B7)). The absence of crossflow must lead to longer swelling compared to conditions of the current SAXS–relaxation experiment where crossflow was present: in experiments, the crossflow partially removed the swelled part of the gel and thus evidently facilitated liquid permeation into the gel from the bulk side [58–61]. This inference is correct when the filtration–consolidation properties of the gel (described by $k(c)\partial\Pi(c)/\partial c$) are equal during filtration and relaxation (i.e. gel compression is fully reversible). According to Eq. (B9), when filtrate can flow across the membrane during the pressure relaxation, a higher R_m equates to a lower swelling rate. In the current study, the local membrane resistance value used (membrane resistance after removing the gel layer, before chemical cleaning) was not measured. However, in order to obtain the lowest estimate for gel swelling rate, Eq. (B9) was used with the value $R_m = 4.9 \cdot 10^{13} \text{ m}^{-1}$, which is the highest value obtained for average membrane resistance after rinsing. Therefore, using this value in Eq. (B9) is a sound overestimation of R_m , which must result in the underestimation of gel swelling rate. The dependency $\Pi(c)$, which is required for the application of Eq. (B9), was taken from the data of Doudiès et al. [43] on the osmotic compression of casein micelle dispersions at 20°C.

The system solution also requires dependency of $k\partial\Pi/\partial c$ on c during the relaxation step. Both k and Π are usually considered as material properties (unique functions of concentration c , and independent of sample history); therefore, the dependency $k\partial\Pi/\partial c$ on c obtained from the analysis of steady-state SAXS–filtration data (as explained in paragraph B1) can be used for modeling the relaxation kinetics (in Eq. (B4)). The modeled and experimental swelling kinetics can then be compared to confirm or discard the assumption that the gel properties ($k\partial\Pi/\partial c$ at a given c) are independent of compression history.

B4. Applicability of proposed analysis of fouling layer properties and swelling kinetics to the studied case of a cell with narrow filter channel

The model of cross-flow filtration developed in Annex A does not account for possible wall effects: lateral (i.e. in y direction, parallel to the membrane surface and perpendicular to the crossflow direction) material (particle, filtrate) fluxes, and/or distribution of shear stress, cross-flow rate, particle concentration, solid pressure, etc. At the same time, our experiments were done in the cell with a narrow (4 mm) but high (8 mm) filter channel (i.e. the width to height ratio was 0.5). It is known that in rectangular ducts with low width to height ratio the cross-flow velocity significantly changes in y direction. Therefore, one may concern about the applicability of our model for the analysis of our experimental data: e.g., $J(x)$ was evaluated instead of $J(x,y)$, or $c(z)$ was discussed instead of $c(y,z)$. Below we briefly justify the model application as well as unnecessary to account for wall effects for our current data analysis and in the following discussion of compression (ir)reversibility.

In the case of a developed laminar flow of Newtonian fluid in a rectangular duct the local crossflow velocity $u(y,z)$ can be obtained with the help of equation provided, for example, in Ref. [63]: $u(y,z)$ is strongly distributed over y , for different z this distribution fits a master curve $u(y,z)/u(0,z)$, which is practically parabolic ($u = 0$ at the lateral walls and u is maximal in the central plane, where $y = 0$). The distribution of a function $[du(y,z)/dz]_{z=0}/[du(y,z)/dz]_{y=0,z=0}$ (i.e. relative shear rate in the direction perpendicular to the membrane, measured on the membrane surface, where $z = 0$) also fits this curve.

As soon as development of the concentration polarization and the deposit growth are impacted by tangential transport of particles, dependency of u on y must result in the dependency of $c(z)$ on y . It can be expected that the slower tangential particle transport in the vicinity of lateral walls of the filter channel results in the faster accumulation of particles in the CP layer and in formation of thicker deposit (in comparison to the central plane, where the crossflow is higher and the particle accumulation must be lower). The increasing of local c from the central plane to the cell walls (i.e. appearance of a gradient $[dc/dy]_z$ due to the decreasing of local u in y direction) must result in lateral diffusion and lateral filtrate permeation. These phenomena will counteract the gradient development and will reduce the wall effect. Nevertheless, in the further calculation of $c(y)$ we will neglect the lateral mass

transport and only consider the “negative” role $u(y)$ in order to evaluate the “worst-case” wall effect.

When the lateral mass transport (diffusion, filtration) is ignored, the local particle transport depends on $u(x,z)$ according to Eq. (A1), which now must be changed to $u(x,y,z)$. It can be demonstrated that transformation of Eq. (A1) containing $u(x,y,z)$ will result in the equation similar to Eq. (A14), but with y -dependent local filtrate flux $J(x,y)$ and $M(y)$:

$$J(x,y)^{-3} = J(0)^{-3} + \frac{3}{2} \frac{c_0 \mu_f^2 x}{M(y)} \quad (\text{B10})$$

Using the definition of M via Eq. (A13), $M(y)$ can be presented as

$$M(y) = M_0 \frac{[du(y,z)/dz]_{z=0}}{[du(y,z)/dz]_{y=0,z=0}} \quad (\text{B11})$$

where M_0 is a constant. In order to obtain Eq. (B11) we assumed a constant viscosity in the CP layer; we expect that such a simplification does not influence the generality of following conclusions. As it was noted above, the function $[du(y,z)/dz]_{z=0}/[du(y,z)/dz]_{y=0,z=0}$ is parabolically distributed over y ; therefore, $M(y)$ has the same strong distribution.

It can be demonstrated that when $J(x,y)$ is much lower than $J(0)$, and x is not too small (as in our experiments), combining Eqs. (B10) and (B11) yields

$$J(x,y) = \left(\frac{3}{2} \frac{c_0 \mu_f^2 x}{M_0} \right)^{-\frac{1}{3}} \cdot \left(\frac{[du(y,z)/dz]_{z=0}}{[du(y,z)/dz]_{y=0,z=0}} \right)^{1/3} \quad (\text{B12})$$

The term in the first brackets of the right-hand side of Eq. (B12) is a constant.

It follows from Darcy’s equation that the deposit height h is inversely proportional to filtrate flux J . The same is true for $h_g(y)$ and $J(y)$, at least, when the lateral diffusion and filtration are neglected. Therefore, distribution of the relative deposit height h_g with y can be obtained from Eq. (B12):

$$\frac{h(x,y)}{h(x,0)} = \left(\frac{[du(y,z)/dz]_{z=0}}{[du(y,z)/dz]_{y=0,z=0}} \right)^{-1/3} \quad (\text{B13})$$

Fig. B2 presents the distribution of the relative deposit height $h(x,y)/h(x,0)$ calculated with the help of Eq. (B13) for the studied case of the width to height ratio of the filter channel equal to 0.5.

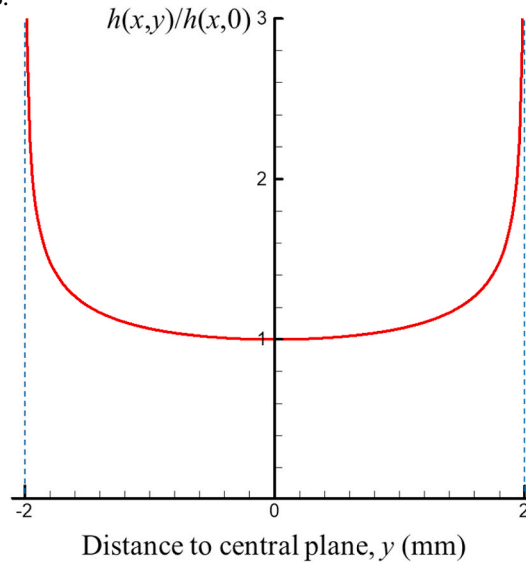


Fig. B2. Relative deposit height $h(x,y)/h(x,0)$ distribution across the filter channel (also, iso-concentration line) calculated via Eq. (B13). Dashed verticals denote cell walls.

The relative deposit height distribution (Fig. B2) is an iso-concentration line $[z(y)/z(0)]_c$, thus it can be used as a measure of the influence of wall effect on a concentration distribution in the deposit and CP layer.

According to Fig. B2, the relative deposit height increases from 1 to 1.2, when y changes from 0 to ± 0.75 . However, further increasing of h near the walls is much stronger. As it was stated above, Fig. B2 presents the result of the worst-case evaluation, which accounts for the crossflow rate distribution (“negative” effect of walls), but neglects lateral diffusion and filtrate flow (“counter-effects” that tend to reduce the inhomogeneity of the lateral concentration distribution). The lateral diffusion and filtration would be more important near the walls, because they would increase with dc/dy , and the latter must increase with $dz(c)/dy$, so, near the walls (Fig. B3). In other words, lateral diffusion will exclude the formation of sharp “horns” of the U-like iso-concentration lines in the CP layer, while lateral filtrate flow will tend to eliminate this “horns” in the deposit.

Nevertheless, moderate influence of the crossflow velocity distribution on the CP layer and deposit formation, i.e. moderate distribution of $[z(y)]_c$ (as compared to that presented in Fig. B2) can be expected. In order to verify its influence on our main data (i.e. measured $c(z)$ curves), in Fig. B3 the $c(z)$ curves obtained during the steady-state of two crossflow filtration experiments (data from Fig. 5) were juxtaposed with a $c(z)$ curve obtained during a dead-end filtration at $\text{TMP} = 1.1$ bar (our unpublished data obtained during the same experimental session using the same suspension, equipment and method as that were used for the crossflow filtration). Since in three studied cases the fouling layers had different thickness and maximal concentration, the $c(z)$ curves were juxtaposed by scaling of z and shifting. This was done for comparison of the local fouling layer structure, which does

not depend on the fouling layer thickness or position (e.g., Eq. (14) in Ref. [64]).

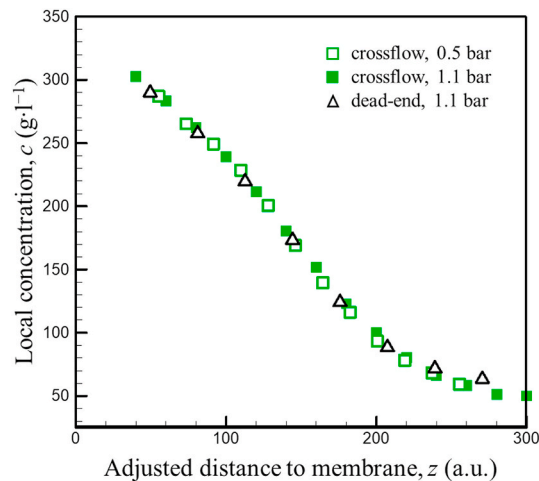


Fig. B3. Dependencies $c(z)$ obtained in crossflow and dead-end filtration experiments after the juxtaposing.

Though experimentally measured $c(z)$ dependencies were not linear and were significantly different, they practically coincided after the appropriate scaling and shifting of z . This means that the same fouling layer structure was obtained at different experimental conditions (crossflow and dead-end filtration). Since, the fouling layer structure obtained during the dead-end filtration was not affected by inhomogeneity of the crossflow velocity by definition (Fig. B3, triangles), then $c(z)$ was also not visually affected by cross-flow inhomogeneity during the crossflow filtration experiments discussed in our current work (Fig. B3, open and filled squares). This justifies our discussion of the data presented in Figs. 3a, 5 and 6 (filtration stage of experiments). While discussion of the data obtained during the pressure relaxation (Fig. 3b) and its comparison with the modeled data (Fig. 7) are independent of the crossflow velocity or its distribution over y .

References

- G. Gésan-Guizou, E. Boyaval, G. Daufin, Critical stability conditions in crossflow microfiltration of skimmed milk: transition to irreversible deposition, *J. Membr. Sci.* 158 (1999) 211–222.
- K.S.Y. Ng, M. Haribabu, D.J.E. Harvie, D.E. Dunstan, G.J.O. Martin, Mechanisms of flux decline in skim milk ultrafiltration: a review, *J. Membr. Sci.* 523 (2017) 144–162.
- B. Espinasse, P. Bacchin, P. Aimar, Filtration method characterizing the reversibility of colloidal fouling layers at a membrane surface: analysis through critical flux and osmotic pressure, *J. Colloid Interface Sci.* 320 (2008) 483–490.
- M.C. Martí-Calatayud, S. Schneider, S. Yüce, M. Wessling, Interplay between physical cleaning, membrane pore size and fluid rheology during the evolution of fouling in membrane bioreactors, *Water Res.* 147 (2018) 393–402.
- P. van der Marel, A. Zwijnenburg, A. Kemperman, M. Wessling, H. Temmink, W. van der Meer, An improved flux-step method to determine the critical flux and the critical flux for irreversibility in a membrane bioreactor, *J. Membr. Sci.* 332 (2009) 24–29.
- S. Schiffer, M. Hartinger, A. Matyssek, U. Kulozik, On the reversibility of deposit formation in low temperature milk microfiltration with ceramic membranes depending on mode of adjustment of transmembrane pressure and wall shear stress, *Separ. Purif. Technol.* 247 (2020) 116962.
- M. Hartinger, S. Schiffer, H.-J. Heidebrecht, J. Dümpler, U. Kulozik, Milk protein fractionation by custom-made prototypes of spiral-wound microfiltration membranes operated at extreme crossflow velocities, *J. Membr. Sci.* 605 (2020) 118110.
- M. Hartinger, S. Schiffer, H.-J. Heidebrecht, J. Dümpler, U. Kulozik, Investigation on the spatial filtration performance in spiral-wound membranes – influence and length-dependent adjustment of the transmembrane pressure, *J. Membr. Sci.* 591 (2019) 117311.
- A. Piry, W. Kühnl, T. Grein, A. Tolkach, S. Ripperger, U. Kulozik, Length dependency of flux and protein permeation in crossflow microfiltration of skimmed milk, *J. Membr. Sci.* 325 (2008) 887–894.
- A. Piry, A. Heino, W. Kühnl, T. Grein, S. Ripperger, U. Kulozik, Effect of membrane length, membrane resistance, and filtration conditions on the fractionation of milk proteins by microfiltration, *J. Dairy Sci.* 95 (2012) 1590–1602.
- N. Wemsy Diagne, M. Rabiller-Baudry, L. Paugam, On the actual cleanability of polyethersulfone membrane fouled by proteins at critical or limiting flux, *J. Membr. Sci.* 425–426 (2013) 40–47.
- U. Kulozik, H.G. Kessler, Rinsing behaviour of deposited layers in reverse osmosis, *Milchwissenschaft* 43 (1988) 784–789.
- T. Steinhauer, J. Lonfat, I. Hager, R. Gebhardt, U. Kulozik, Effect of pH, transmembrane pressure and whey proteins on the properties of casein micelle deposit layers, *J. Membr. Sci.* 493 (2015) 452–459.
- C. Martin, F. Pignon, A. Magnin, M. Meireles, V. Lelièvre, P. Lindner, B. Cabane, Osmotic compression and expansion of highly ordered clay dispersions, *Langmuir* 22 (2006) 4065–4075.
- P. Bacchin, P. Aimar, R.W. Field, Critical and sustainable fluxes: theory, experiments and applications, *J. Membr. Sci.* 281 (2006) 42–69.
- A.J.E. Jimenez-Lopez, N. Leconte, O. Dehainault, C. Geneste, L. Fromont, G. Gésan-Guizou, Role of milk constituents on critical conditions and deposit structure in skimmed milk microfiltration (0.1 μm), *Separ. Purif. Technol.* 61 (2008) 33–43.
- P. Qu, G. Gésan-Guizou, A. Bouchoux, Dead-end filtration of sponge-like colloids: the case of casein micelle, *J. Membr. Sci.* (2012) 417–418, 10–19.
- P. Qu, A. Bouchoux, G. Gésan-Guizou, On the cohesive properties of casein micelles in dense systems, *Food Hydrocolloids* 43 (2015) 753–762.
- M.H. Nogueira, G.M. Tavares, N.F. Nogueira Silva, F. Casanova, P.C. Stringheta, F. Gaucheron, A.V.N.C. Teixeira, I.T. Perrone, A.F. Carvalho, Physico-chemical stability of casein micelles cross-linked by transglutaminase as a function of acidic pH, *Food Struct.* 19 (2019) 100103.
- P. Bacchin, P. Aimar, V. Sanchez, Model for colloidal fouling of membranes, *AIChE J.* 41 (1995) 368–376.
- P. Harmant, P. Aimar, Coagulation of colloids retained by porous wall, *AIChE J.* 42 (1996) 3523–3532.
- P. Bacchin, D. Si-Hassen, V. Starov, M.J. Clifton, P. Aimar, A unifying model for concentration polarization, gel-layer formation and particle deposition in cross-flow membrane filtration of colloidal suspensions, *Chem. Eng. Sci.* 57 (2002) 77–91.
- P. Aimar, P. Bacchin, Slow colloidal aggregation and membrane fouling, *J. Membr. Sci.* 360 (2010) 70–76.
- E. Iritani, N. Katagiri, G. Inagaki, Compression and expansion properties of filter cake accompanied with step change in applied pressure in membrane filtration, *Separ. Purif. Technol.* 198 (2018) 3–9.
- M. Loginov, F. Samper, G. Gésan-Guizou, T. Sobisch, D. Lerche, E. Vorobiev, Centrifugal ultrafiltration for determination of filter cake properties of colloids, *J. Membr. Sci.* 536 (2017) 59–75.
- E. Iritani, N. Katagiri, T. Yoshida, Simplified evaluation of consolidation and expansion behaviour of highly compressible cake, *Filtration* 18 (2018) 50–60.
- M. Iwata, T. Murase, Expansion and stress relaxation of expressed cake, *Dry. Technol.* 11 (1993) 749–767.
- T. Murase, M. Iwata, M. Wakita, T. Adachi, N. Hayashi, M. Shirato, Expansion of consolidated material after release of load, *J. Chem. Eng. Jpn.* 22 (1989) 195–199.
- A. Bouchoux, P. Qu, P. Bacchin, G. Gésan-Guizou, A general approach for predicting the filtration of soft and permeable colloids: the milk example, *Langmuir* 30 (2014) 22–34.
- C. Guell, M. Ferrando, F. Lopez (Eds.), *Monitoring and Visualizing Membrane-Based Processes*, Wiley, 2009.
- V. Chen, H. Li, A.G. Fane, Non-invasive observation of synthetic membrane processes – a review of methods, *J. Membr. Sci.* 241 (2004) 23–44.

- [32] F. Pignon, G. Belina, T. Narayanan, X. Paubel, A. Magnin, G. Gésan-Guiziou, Structure and rheological behavior of casein micelle suspensions during ultrafiltration process, *J. Chem. Phys.* 121 (2004) 8138–8146.
- [33] C. David, F. Pignon, T. Narayanan, M. Sztucki, G. Gésan-Guiziou, A. Magnin, Spatial and temporal in-situ evolution of concentration profile during casein micelle ultrafiltration probed by SAXS, *Langmuir* 24 (2008) 4523–4529.
- [34] Y. Jin, N. Hengl, S. Baup, F. Pignon, N. Gondrexon, M. Sztucki, G. Gésan-Guiziou, A. Magnin, M. Abyan, M. Karrouch, D. Blésès, Effects of ultrasound on cross-flow ultrafiltration of skim milk: characterization from macro-scale to nano-scale, *J. Membr. Sci.* 470 (2014) 205–218.
- [35] Y. Jin, N. Hengl, S. Baup, G. Maitrejean, F. Pignon, Modeling and analysis of concentration profiles obtained by in-situ SAXS during cross-flow ultrafiltration of colloids, *J. Membr. Sci.* 528 (2017) 34–45.
- [36] F. Pignon, M. Abyan, C. David, A. Magnin, M. Sztucki, In-situ characterization by SAXS of concentration polarization layers during cross-flow ultrafiltration of Laponite dispersions, *Langmuir* 28 (2012) 1083–1094.
- [37] E.F. Semeraro, N. Hengl, M. Karrouch, L.J. Michot, E. Paineau, B. Jean, J.L. Putaux, C. Lancelon-Pin, L. Sharpnack, F. Pignon, Layered organization of anisometric cellulose nanocrystals and beidellite clay particles accumulated near the membrane surface during cross-flow ultrafiltration: in situ SAXS and ex situ SEM/WAXD characterization, *Colloids Surf., A* 584 (2020) 124030.
- [38] Y. Jin, N. Hengl, S. Baup, F. Pignon, N. Gondrexon, M. Sztucki, A. Romdhane, A. Guillet, M. Auroousseau, Ultrasonic assisted cross-flow ultrafiltration of starch and cellulose nanocrystals suspensions: characterization at multi-scales, *Carbohydr. Polym.* 124 (2015) 66–76.
- [39] C. Rey, N. Hengl, S. Baup, M. Karrouch, A. Dufresne, H. Djeridi, R. Dattani, F. Pignon, Velocity, stress and concentration fields revealed by micro-PIV and SAXS within concentration polarization layers during cross-flow ultrafiltration of colloidal Laponite clay suspensions, *J. Membr. Sci.* 578 (2019) 69–84.
- [40] C. Rey, N. Hengl, S. Baup, M. Karrouch, E. Gicquel, A. Dufresne, H. Djeridi, R. Dattani, Y. Jin, F. Pignon, Structure, rheological behavior and in-situ local flow fields of cellulose nanocrystal dispersions during cross-flow ultrafiltration, *ACS Sustain. Chem. Eng.* 7 (2019) 10679–10689.
- [41] M.H. Famelart, F. Lepesant, F. Gaucheron, Y. Le Graet, P. Schuck, pH-induced physicochemical modifications of native phosphocaseinate suspensions: influence of aqueous phase, *Lait* 76 (1996) 445–460.
- [42] C. Gaiani, J. Scher, P. Schuck, J. Hardy, S. Desobry, S. Banon, The dissolution behaviour of native phosphocaseinate as a function of concentration and temperature using a rheological approach, *Int. Dairy J.* 16 (2006) 1427–1434.
- [43] F. Doudiès, A.-S. Arsène, F. Garnier-Lambrouin, M.-H. Famelart, A. Bouchoux, F. Pignon, G. Gésan-Guiziou, Major role of voluminosity in the compressibility and sol-gel transition of casein micelle dispersions concentrated at 7 °C and 20 °C, *Foods* 8 (2019) 652–671.
- [44] S. Nobel, K. Weidendorfer, J. Hinrichs, Apparent voluminosity of casein micelles determined by rheometry, *J. Colloid Interface Sci.* 386 (2012) 174–180.
- [45] J.L. Gaddis, Effects of pressure and crossflow velocity on ultrafiltration flux, *Chem. Eng. Commun.* 116 (1992) 153–169.
- [46] T. Tanaka, D.J. Fillmore, Kinetics of swelling of gels, *J. Chem. Phys.* 70 (1979) 1214–1218.
- [47] M. Loginov, F. Doudiès, N. Hengl, F. Pignon, G. Gésan-Guiziou, Influence of membrane resistance on swelling and removal of colloidal filter cake after filtration pressure release, *J. Membr. Sci.* 595 (2020) 117498.
- [48] M. Rabiller-Baudry, M. Le Maux, B. Chaufer, L. Begoin, Characterisation of cleaned and fouled membrane by ATR-FTIR and EDX analysis coupled with SEM: application to UF of skimmed milk with a PES membrane, *Desalination* 146 (2002) 123–128.
- [49] F.M. Tiller, J.H. Kwon, Role of porosity in filtration: XIII. Behavior of highly compactible cakes, *AIChE J.* 44 (1998) 2159–2167.
- [50] M. Iwata, S. Koda, H. Nomura, Theory of compression and expansion of hydrogels, *J. Chem. Eng. Jpn.* 32 (1999) 684–688.
- [51] T. Murase, M. Iwata, T. Adachi, Expansion of inhomogeneous cake after release of load, *J. Chem. Eng. Jpn.* 23 (1990) 108–110.
- [52] T. Murase, M. Iwata, T. Adachi, M. Wakita, Stress relaxation of expressed cake, *J. Chem. Eng. Jpn.* 22 (1989) 655–659.
- [53] M. Elimelech, S. Bhattacharjee, A novel approach for modeling concentration polarization in crossflow membrane filtration based on the equivalence of osmotic pressure model and filtration theory, *J. Membr. Sci.* 145 (1998) 223–241.
- [54] C. Tien, *Principles of Filtration*, Elsevier, London, 2012.
- [55] J. Olivier, J. Vaxelaire, E. Vorobiev, Modelling of cake filtration: an overview, *Separ. Sci. Technol.* 42 (2007) 1667–1700.
- [56] E. Höfgen, S. Kühne, U.A. Peuker, A.D. Stickland, A comparison of filtration characterisation devices for compressible suspensions using conventional filtration theory and compressional rheology, *Powder Technol.* 346 (2019) 49–56.
- [57] A.D. Stickland, C. Burgess, D.R. Dixon, P.J. Harbour, P.J. Scales, L.J. Studer, S. P. Usher, Fundamental dewatering properties of wastewater treatment sludges from filtration and sedimentation testing, *Chem. Eng. Sci.* 63 (2008) 5283–5290.
- [58] H. Xin, X.D. Chen, N. Özkan, Removal of a model protein foulant from metal surfaces, *AIChE J.* 50 (2004) 1961–1973.
- [59] P. Valois, E. Verneuil, F. Lequeux, L. Talini, Understanding the role of molar mass and stirring in polymer dissolution, *Soft Matter* 12 (2016) 8143–8154.
- [60] A. Briffaz, P. Bohuon, J.M. Méot, B. Matignon-Pons, C. Mestres, Modelling of water transport with convection effects on amylose transfer in a swelling, eroding and gelatinizing starchy matrix, *J. Food Eng.* 221 (2018) 132–140.
- [61] D.E. Rosner, Lifetime of a highly soluble dense spherical particle, *J. Phys. Chem.* 73 (1969) 382–387.
- [62] F. Doudiès, M. Loginov, N. Hengl, M. Karrouch, N. Leconte, F. Garnier-Lambrouin, J. Pérez, F. Pignon, G. Gésan-Guiziou, Build-up and relaxation of membrane fouling deposits produced during crossflow ultrafiltration of casein micelle dispersions at 12 °C and 42 °C probed by in situ SAXS, *J. Membr. Sci.* 618 (2021) 118700.
- [63] F. White, *Viscous Fluid Flow*, McGraw-Hill, New York, 2006, p. 112.
- [64] E. Iritani, Properties of filter cake in cake filtration and membrane filtration, *KONA* 21 (2003) 19–39.